TALLINNA TEHNIKAÜLIKOOL
TALLINN UNIVERSITY OF TECHNOLOGY

Department of Materials and Environmental Technology

DEPOSITION AND PROPERTIES OF MoO_3 FOR HYBRID SOLAR CELLS

MOO_3 SADESTUS JA OMADUSED RAKENDAMISEKS HÜBRIIDPÄIKESEELEMENTID

Master Thesis

Jude Awele Okolie

Student code 166450KAYM

Supervisor Atanas Katerski, Researcher,

Laboratory of Thin Film Chemical Technologies, Department of Materials and Environmental Technologies.

Tallinn, 2018

AUTHOR'S DECLARATION

Hereby I declare, that I have written this thesis independently.

No academic degree has been applied for based on this material. All works, major viewpoints and data of the other authors used in this thesis have been referenced.

"....." ..... 201.....

Author: Jude Awele Okolie

/signature /

Thesis is in accordance with terms and requirements

"....." ..... 201....

Supervisor: Atanas Katerski

/signature/

Accepted for Defence

"....."..... 201... .

Chairman of theses defence commission: .....

/name and signature/

TTÜ Department of Materials and Environment Technology

THESIS TASK

Student: Jude Awele Okolie, 166450KAYM

Study programme: KAYM, Materials and Process of Sustainable energetics

Main Speciality: Process of Sustainable Energetics

Supervisor(s): Dr. Atanas Katerski, Researcher, +3726203369

Thesis topic:

(in English) *Deposition and properties of MoO_3 for hybrid solar cells*

(in Estonian) *MoO_3 sadestus ja omadused rakendamiseks hübriidpäikeseelementid*

Thesis main objectives:

1. To fabricate MoO_3 thin films using vacuum thermal deposition methods.

2. To determine the structural and optical properties of vacuum deposition MoO_3 thin films which is to be used as an interfacial buffer layer for hybrid solar cells.

3. To ascertain if MoO_3 thin films is a suitable interfacial buffer layer for hybrid solar cell.

Thesis tasks and time schedule:

No	Task description	Deadline
1.	Deposit MoO_3 on glass substrate using vacuum thermal evaporation method	
2.	Thermal annealing of produced MoO_3 films at different temperatures	
3	Characterize the properties of as – deposited films and films annealed at different temperatures by UV – VIS, XRD, SEM and EDX.	
4.	Evaluate the performance of the as deposited MoO_3 films as interfacial layer in hybrid solar cells ITO/TiO_2/Sb_2S_3/P_3HT/MoO_3/Au against a reference solar cell ITO/TiO_2/Sb_2S_3/P_3HT/ Au	

Language: English…… **Deadline for submission of thesis:** "...05...."....June.....2018….

Student: Jude Awele Okolie ..... "....."....201….a

/signature/

Supervisor: Atanas Katerski ..... "....."....201….a

/signature/

Table of contents

PREFACE

Before you lies the thesis titled “Deposition and properties of MoO_3 for hybrid solar cells”. The project involves the production of MoO_3 thin films via vacuum thermal evaporation and the characterization of the thin films to determine its suitability as interfacial buffer layer for an inverted hybrid solar cell. This thesis has been meticulously written to fulfil the graduation requirements of the Masters of Engineering Degree in Materials and Sustainable Energetics Programme at Tallinn University of Technology, Estonia.

This work is financially supported by the Estonian Ministry of Education and Research projects IUT 19-4 and by the European Union through the European Regional Development Fund “Centre of Excellence” project TK141: “Advanced materials and high-technology devices for sustainable energetics, sensorics and nanoelectronics”. I would like to thank Dr. Valdek Mikli for the SEM and EDX measurements.

I also want to thank everyone who supported me during my Master’s degree journey at Tallinn University of Technology. Firstly, I appreciate the Almighty benign God in his infinite mercy for his grace and strength to see me through during trying times. I am thankful to my late father Mr. Peter Okolie. His advice, constructive criticism and support soared me to greater success.

My deepest appreciation goes to my Supervisor, Dr. Atanas Katerski, who helped me with his professional expertise and suggestions. Above all, he never gave up on me, his patience and teaching skills was impeccable, I couldn’t have done this all alone without him.

Also, my sincere gratitude also goes to the Estonian government and Tallinn University of Technology for supporting my studies and research through the tuition waiver scholarship, Dora scholarship, Speciality scholarship, Needs based scholarship and Performance scholarships. Those grants were invaluable towards the successful completion of my studies. I am grateful to the course Director, Professor Andres Öpik, and all the members of the laboratory of thin film chemical technology at Tallinn University of Technology for their understanding and support during the phase of my project. Finally, I want to appreciate all my friends, family members and classmates who has supported me throughout my stay in Estonia.

Jude Awele Okolie

List of abbreviations, terminologies and acronyms

a, b, c and h, k, l	Lattice parameters
CO_2	Carbon dioxide
d_{khl}	Plane spacing values related to the Miller indices
EDX	Energy dispersive X-ray spectroscopy
Eg	Optical energy band gap
ETL	Electron transport layers
FF	Fill factor
HTL	Hole transport layers
J_{SC}	Short circuit current
M1 –M6	As- deposited films and films heated at 150, 200, 300, 400 and 500 ^{o}C respectively
MoO_3	Molybdenum oxide
N_2	Nitrogen
OPV	Organic photovoltaics
PCE	Power conversion efficiency
PEDOT:PSS	Poly(3,4-ethylenedioxythiophene) polystyrene sulfonate
PV	Photovoltaics
P3HT	Poly(3-hexylthiophene 2,5-diyl)
SC	Solar cells
SEM	Scanning electron microscopy
V_{OC}	Open circuit voltage
XRD	X-Ray Diffraction

INTRODUCTION

Over the last decade , the emission of carbon dioxide (CO_2) and other obnoxious gases that promote global warming has increased tremendously as a result of the continual usage of coal, natural gas, and petroleum resources [1]. In the event of the accelerating impact of greenhouse gases coupled with the depleting nature of fossils fuels, there is an urgent need to explore renewable and sustainable sources of energy for societal and industrial benefits. Wind, biomass, hydro power, solar power and geothermal are renewable energies that has been widely explored to compliment the usage of fossils. However, of all the renewable energy sources only solar, geothermal and biomass can be used to produce adequate heat energy needed for power generation [2]. Most interestingly, solar power exhibits the highest worldwide potential of all the three since biomass is not present everywhere in nature and geothermal sources are restricted to only few locations [3].

Solar energy is the energy from the sun produced for the earth. Hypothetically solar energy has the potential to satisfy the energy demand of the whole world with almost four million exajoules (1 E*J* = 10^{18}J) of sunlight energy reaching the earth surface yearly [4]. Photovoltaic (PV) Solar cells convert sunlight into a clean and reliable renewable energy sources. In the early years silicon (Si) solar cells has been dominant in the PV market. This is largely due to the abundance of Si, environmental benign nature and high stable cell efficiencies together with the tons of readily available skills related to silicon devices [5]. However, despite the benefits of Si solar cells, high cost due to purification and manufacturing techniques is still a major challenge that slows down the progress of monocrystalline Si. In an attempt to reduce the manufacturing cost of solar cells by eliminating the use of Si materials thin films are used [6].Nevertheless, thin films solar cells are characterized by limited stability, technological challenges and a relatively small market share [7] . This limitation brought about an interest in the third generation solar cells.

The third generation solar cells comprises of the dye-sensitized solar cells (DSSCs), organic and inorganic solar cells, polymer cells and quantum dot cells [8]. Conventional solar cells produced from inorganic material offers high efficiency [9], they can also be produced as nanoparticles, these gives them distinct features such as high absorption coefficient and size tunability. However, their usage is limited due to the high cost of inorganic materials coupled with the energy intensive processing methods [10]. Recently there has been renewed interest in the use of organic materials for photovoltaic applications. Solar cells made from organic materials are inexpensive and their properties can be adjusted by chemical synthesis

and molecular design [10]. Organic solar cells can also be produced using phase technologies such as ink jet printing or various roll to roll techniques, which makes them relatively cheap [11,12]. This offers significant benefits compared to the expensive inorganic solar cells. In order to solve the challenges of inorganic solar cells, new methods of producing cost effective and high efficiency solar cells that combines the unique features of inorganic materials with the thin film forming properties of organic materials is invaluable. Hybrid solar cells are produced by combining organic and inorganic materials, they are cheap alternatives to conventional solar cells. Hybrid solar cells are manufactured with the possibility of utilising the inexpensive and cost effective production of organic solar cell materials together with other benefits such as tuneable absorption spectra from the inorganic component. Despite the immense benefits observed in hybrid solar cells their efficiencies are quite low, also they have a limited lifetime and stability [13]. To prolong the lifetime of Hybrid solar cells, increase their efficiency and obtain the desired stability needed for commercial applications interfacial buffer layers are used. Buffer layers prevents the diffusion of the cathode materials into the active layers thereby enhancing the stability of the solar cells and it also helps to smoothen the anode and surface [14]. PEDOT: PSS is the most commonly used anode buffer layer in hybrid solar cells, however its hygroscopic and acidic nature (leading to organic solar cell degradation in ambient conditions) also its inhomogeneous electric properties is still a major challenge [15,16]. So far it has been unsuccessful Substituting the PEDOT: PSS layer and other interfacial layers in maintaining the required conversion efficiencies due to the high resistance possessed by the interfacial layers. Also, the use of high vacuum deposition technique to deposit the low work function electrodes in conventional hybrid solar cells tends to increase fabrication cost. A good alternative to alleviate the problem is to use a PEDOT: PSS free inverted device structure in which the polarity of the electrode collecting the charge is reversed [17] . In that way, electrons can be extracted from the transparent cathode and holes at the anode thereby enhancing the device stability and lifetime [18]. Also, the inverted architecture saves cost by using non-vacuum deposited metal electrode at the top interface [19]. Nevertheless, the performance of an inverted solar cell is still dependent on the interfacial buffer layer, which should be electrically conductive and transparent [17]. Choosing a suitable interfacial buffer layer for an inverted solar cell in order to optimize its performance is an issue that needs further attention.

A number of studies has reported the use of metal oxides as interfacial buffer layers for solar cells [17,18,20,21]. Recently Molybdenum oxide (MoO_3) thin films has drawn more attention as an interfacial buffer layer for hybrid solar cells due to its interesting optical, chemical and electronic properties [22–

25]. MoO_3 has a wide band gap, layered structure and it also exhibits multiple valence states and characterized by high transmittance and high work function [26].The use of thermally evaporated MoO_3 in hybrid solar cells shows increased lifetime and comparable performance to that of PEDOT:PSS [27]. MoO_3 serves as a protective layer against atmospheric oxygen and humidity. In addition, decreases hole recombination at the electrodes due to its unique electronic properties [27].

Conversely it is important to optimize the growth conditions of MoO_3 and produce pure thin films with precise morphology, structure and optical properties for hybrid solar cells [28]. An understanding of the composition, structure and properties of MoO_3 thin films is of immense importance in the optimization of the growth conditions. The aim of this research is to investigate for the first time the composition, structural and optical properties of vacuum deposited MoO_3 as a protective layer for hybrid solar cells and investigate the effect of thermal annealing on the structural and optical properties of the produced MoO_3 thin films. Furthermore, we compared the performance of MoO_3 as a protective layer for an inverted solar cell with device configuration of ITO/TiO_2/Sb_2S_3/P_3HT/MoO_3/Au against a reference solar cell ITO/TiO_2/Sb_2S_3/P3HT/ Au. The novelty of this work lies in the fact that no study has reported the use of MoO3 as an interfacial buffer layer for an inverted hybrid solar cell with configuration ITO/TiO_2/ Sb_2S_3/P_3HT/ MoO_3/Au.

The thesis is organized as follows:

Chapter I provides an up-to date literature review with a focus on the characteristics of solar cells and the evolution of solar cells from first to third generations of solar cells with lucid examples. Furthermore, the evolution of hybrid solar cell is introduced together with the structure and working principles, an overview of the advantages and limitations of organic and inorganic materials is also discussed. Additionally, the structure of MoO_3 as interfacial layer in hybrid solar cell is also described and different thin film deposition methods are discussed. Finally, the aim and scope of this thesis is elucidated.

Chapter II Describes the experimental methodology used in the deposition of MoO_3 on glass substrate as well as the method of characterization. The vacuum thermal evaporation method was used with a detail description provided. Also, a general description of each characterization method used is described.

Chapter III Critical analysis of the experimental results and discussion.

Chapter IV Presents the conclusions and recommendations for future work.

CHAPTER I: LITERATURE REVIEW

1.1 Photovoltaic solar cells

Solar cells convert sunlight energy into electrical power. The electrical power is defined as the product of electric current (I) and electrical voltage or electrical potential (V). The two main functions of a solar cells are: generation of a photovoltage and photocurrent generation [29]. Solar cells operate on the principle of photovoltaic effect. A semiconductor is used as a light absorber to convert photons from sunlight into an electron-hole pair (Photocurrent generation). The holes and electrons are then separated by the device structure. Electrons migrate to the negative terminals while the holes move to the positive terminals thus producing electric power [30]. Charge separation inside the solar cells leads to the generation of a photovoltage. The working principle of a modern solar cell is illustrated in Figure 1.1: Photon absorption occurs throughout the silicon crystal wafer and extends outside the depletion region while the charge separation involves diffusion of photo-excited charge carriers towards the depletion region.

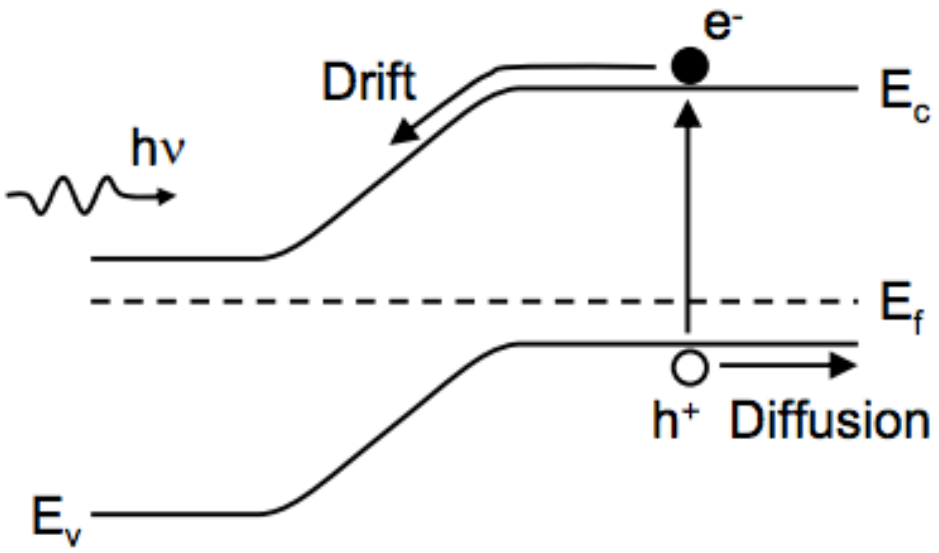

Figure 1.1 : Working principles of Si solar cells [Adapted from ref [31]].

A schematic representation of a solar cell under illumination is presented in Figure 1.2 [31]. Light releases photons from the covalent bonds holding the semiconductor together by entering the gaps between the top contact metal. Mobile charge carriers of the same polarity within the cells are aligned and they move in the same direction with the aid of a p-n junction within the cell. Flow of electrons will complete the circuit and electrical current would be produced if an electric load, such as a lamp is connected between the top and rear contacts of the cell [31] .

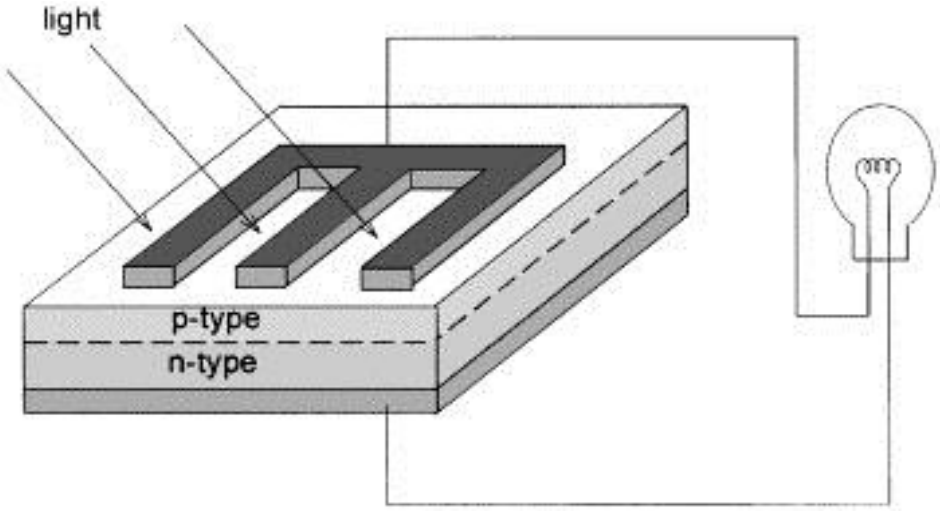

Figure 1. 2 : Energy from sunlight is absorbed and converted into electrical current flow in a load such as a lamp connected between the cell contacts [adapted from ref. [31]].

1.1.1 Characteristics of solar cells

The basic characteristics of the solar cells are the short circuit current (J_{SC}), open circuit voltage (V_{OC}), the fill factor (FF) and the power conversion efficiency (PCE). These parameters are used to ascertain the performance of solar cells. Short circuit current refers to the current produced under illumination without the influence of any external potential. When there is no current flowing through the terminals of the solar cells under illumination, a potential difference exists. This potential difference is known as the open circuit voltage. Fill factor is defined as the ratio of maximum power generated by the solar cell to the product of short circuit current and open circuit voltage. The solar energy conversion efficiency is the ratio of maximum power generated by the solar cell to the energy of incident radiation. Figure 1.3, shows the current voltage characteristics of a solar cell with and without illumination. The short circuit current (J_{sc}), open circuit voltage (V_{oc}) and fill factor (FF) are identified in the figure 3 [32].

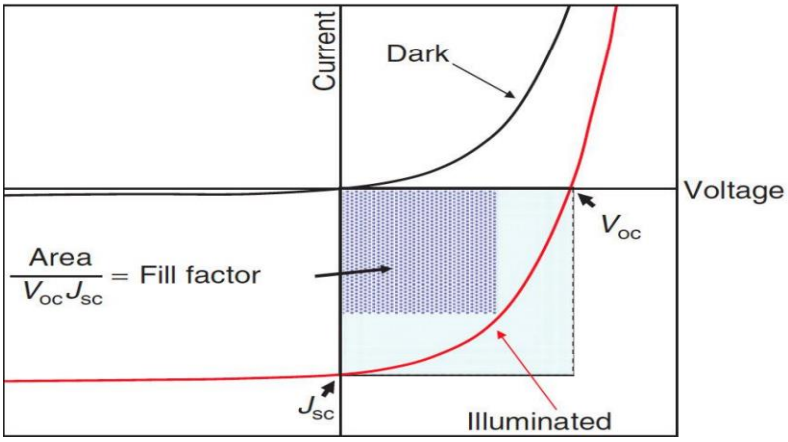

Figure 1. 3: Current voltage characteristics of a solar cell with and without illumination [adapted from ref. [32]].

1.1.2 Photovoltaic solar cell evolution.

The first generation solar cells are based on silicon wafer, they are mainly single crystals and bulk polycrystalline silicon wafers. They provide solar conversion efficiencies 16- 21% (Figure 1.4) depending on the quality of the wafer and the manufacturing techniques.

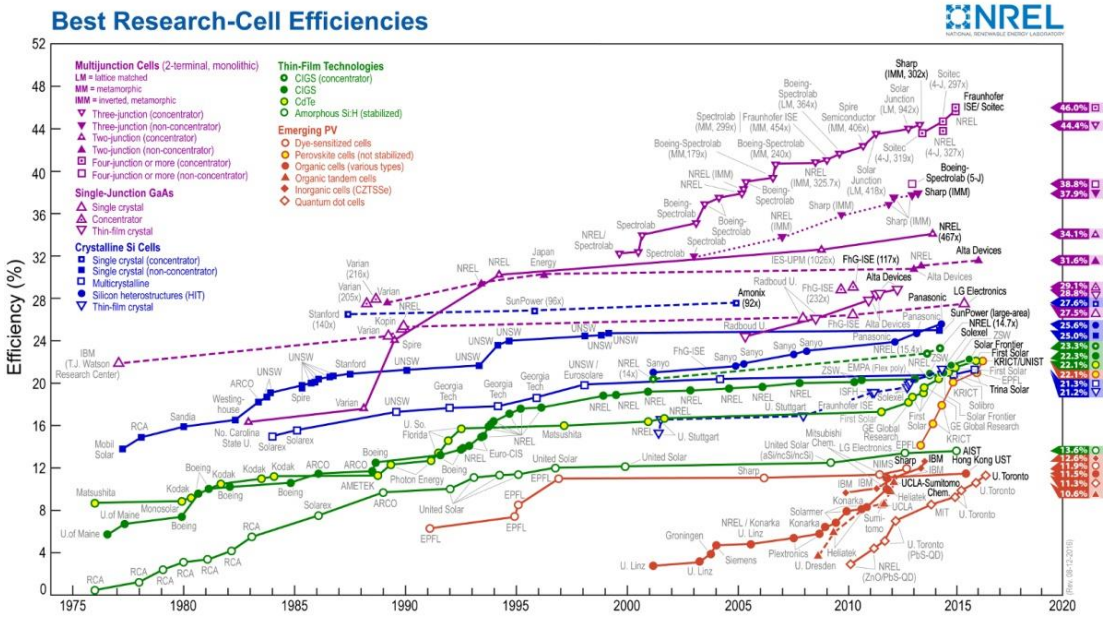

Figure 1. 4 : Efficiency of different generation of solar cells [adapted from ref. [33]].

Polycrystalline silicon materials are used to replace single crystal silicon materials due to their high cost and sophisticated technological steps involved in the use of single silicon wafer. The second generation solar cells are made from thin films [34]. Thin film technology involves the deposition of thin layers of semiconductor materials on a supporting substrate such as a large glass sheet [31] (Figure 4). Thin film technology requires semiconductor materials with thickness of about 100-10000 times less than that of a silicon wafer. The technology also offers potential cost reduction in manufacturing process compared to the first generation solar cells. In addition, thin layer solar cells require flexible substrates, low temperature processes integrated cell insulation and high automation level in series production. This attributes lowers their production cost and enhances the probability of this solar cells to participate effectively in the energy conversion sector [34]. In thin film solar cells virtually any semiconductor material can be used due to the reduced material requirements. There is also a wide range of semiconductor materials to select from since semiconductors can be formed from single elemental atoms, alloys involving multiple elements and compounds [35]. Cadmium sulphide device dominated the early years of thin film technologies until its stability were perceived insolvable [33]. Some other examples of thin film materials includes copper–indium–gallium–selenide (CIGS) and related compounds, cadmium telluride (CdTe) [33].

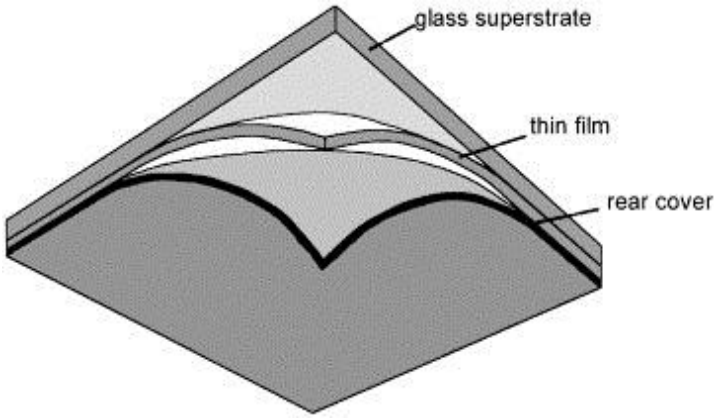

Figure 1. 5: Thin film technology approach [adapted from ref. [33]].

Majority of the third generation solar cells comprises of the dye-sensitized solar cells (DSSCs), organic and inorganic solar cells, polymer cells and quantum dot cells [8]. Their sole aim is to increase device efficiency which is one of the demerits of second generation solar cells and also to reduce cost which is one of the disadvantages of the first generation solar cells [8]. Figure 1.6 elucidates different generations of solar cells.

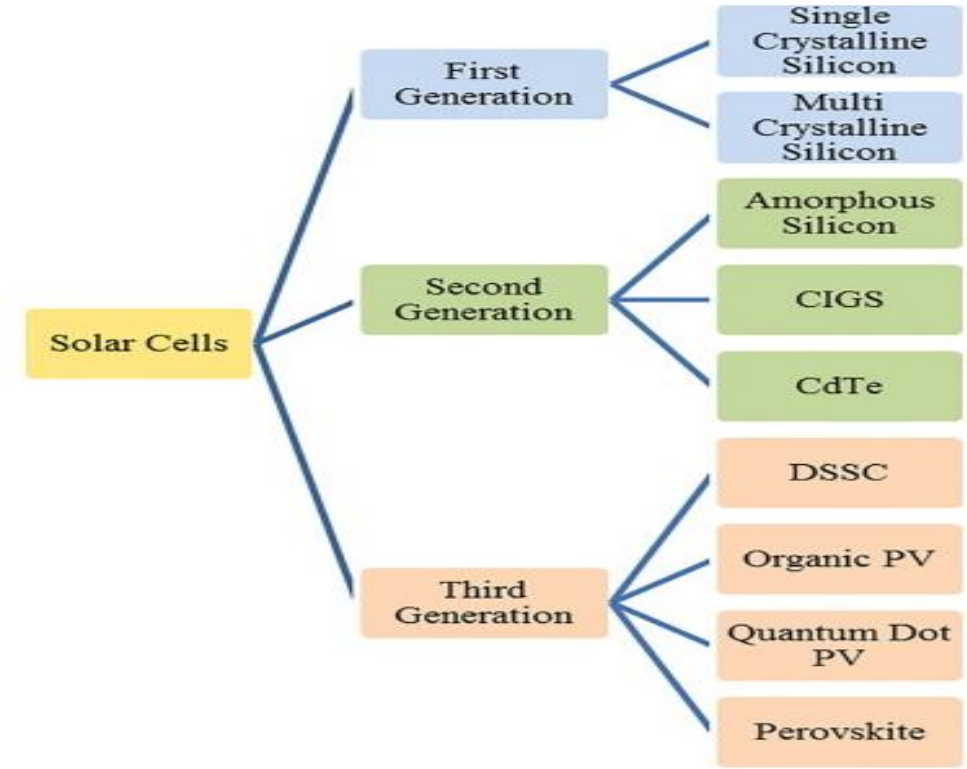

Figure 1. 6: Different generations of solar cells [adapted from ref. [8]].

1.2 Hybrid solar cells.

In the 20th century, the advancement in material developments in the nanometer scale led to the generation of new photovoltaic materials and devices, one of which is the electrochemical dye-sensitized solar cell (DSSC). Grätzel and co-workers were credited for the revolutionary development of the DSSC in 1991 [36]. In this type of solar cell, nanostructured TiO_2 is sensitized by a monolayer of an organic dye as shown in figure 1.7. The DSSC consists of an electrochemical system sandwiched between a counter electrode and a photo anode. However, due to the short lifetime, the electrochemical hole

conductor was replaced with a solid hole conductor in DSSC. Later, the organic dye was also replaced with an inorganic absorber material which gives rise to hybrid solar cell.

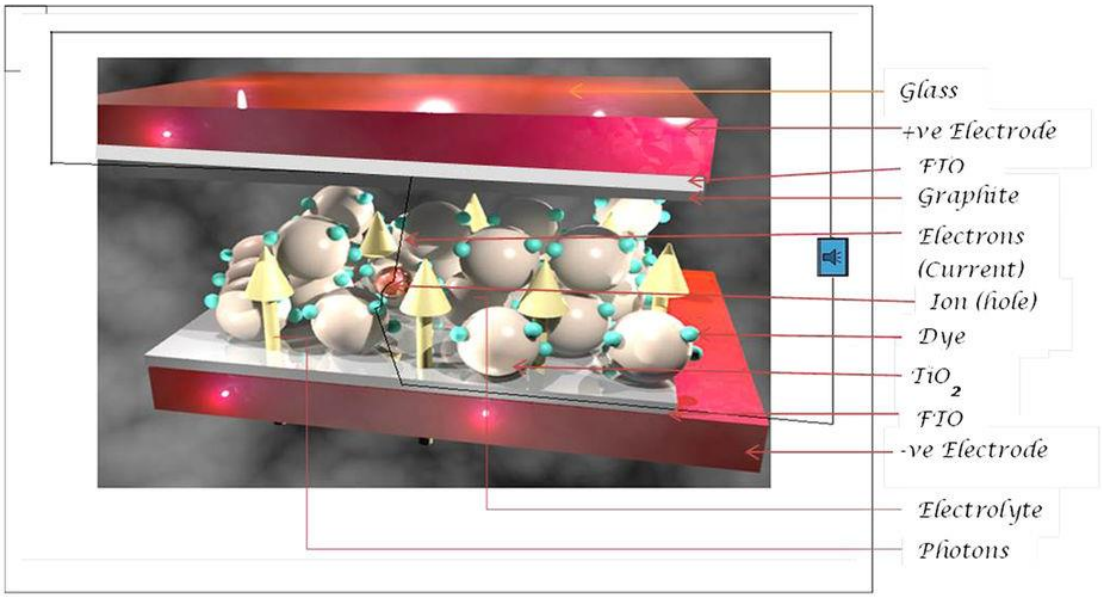

Figure 1. 7: Structure of a typical dye sensitized solar cell [Adapted from ref [37].

Organic-inorganic hybrid solar cells combines the unique features of both organic and inorganic materials. The advantages of organic solar cells includes their low manufacturing cost, easy fabrication method, high processing speed and excellent mechanical properties [38, 39]. Despite the immense benefits of organic solar cells some challenges still exist. For instance during the preparation of the conjugated polymers in organic solar cells the solvents used are usually hazardous and not environmental friendly [39]. Also, the issues of low power conversion efficiency and poor operational stability is still unsolved [38]. On the contrary, inorganic materials are environmental friendly, improved light absorption spectra, quantum confinement advantages and ultrafast induced charge carriers [40]. In hybrid organic- inorganic solar cells organic materials (usually the conjugated polymer) is combined with inorganic nanoparticles with the aim of utilizing the benefits associated with both material groups [40,41]. In that way the low cost of materials of the organic section can be maintained while the inorganic part provides further advantages to the solar cells [40]. Incorporating organic and inorganic materials in solar cells provides lots of benefits. Firstly, inorganic materials are more environmentally benign compared to the organic counterparts therefore the additional of the material to organic materials would help prevent the photo induced degradation of conjugated organic semiconductors.

Secondly, light absorption in organic material is greater than that of the organic materials [42]. Lastly it is generally perceived that the inorganic quantum dots produce ultra-fast induced charge carriers to organic materials. The next section introduces the structure and working principle of a typical organic-inorganic hybrid solar cell.

1.2.1 Device structure and Working principle of Organic- Inorganic Hybrid solar cells

A typical hybrid solar cells consists of thin film devices with photoactive layers sandwiched between two electrodes having different work functions. The anode typically consists of transparent and highly conductive indium tin oxide deposited on a flexible glass substrate. The function of the anode is to allow the passage of light through the material and collect holes from the device. The photoactive layers consist of both organic and inorganic part. A metal cathode electrode made of either Al, LiF/Al, Ca/Al is vacuum deposited on the top of the photoactive layer. The cathode collects electrons from the device and the layer is usually deposited via thermal evaporation. Schematic representation of a typical organic – inorganic hybrid solar cell is shown in figure 1.8 [43].

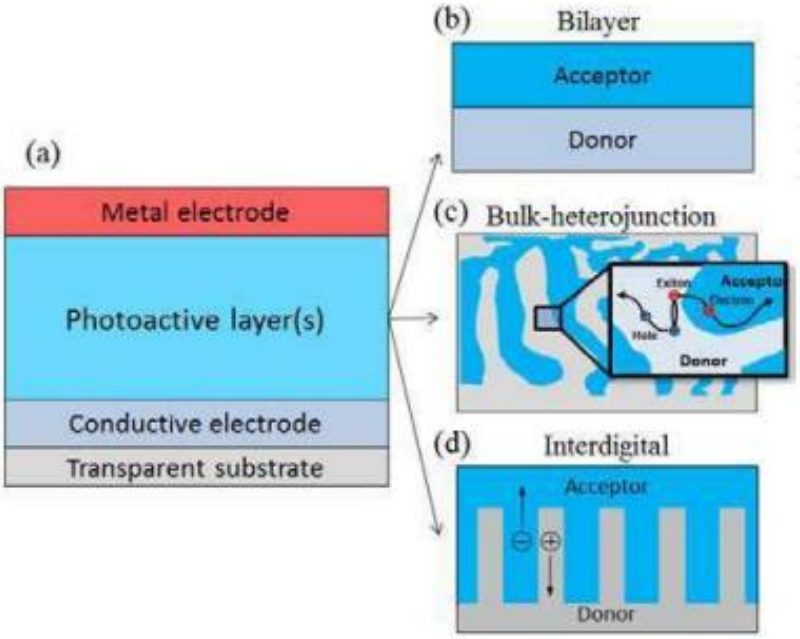

Figure 1. 8: Schematic representation of a typical Organic - Inorganic Hybrid solar cells [43].

The photoactive layers usually exist in two different structures; the bilayer structure and the bulk heterojunction structure as shown in Figure 1. 8. The bulk heterojunction structure is obtained by just bending the acceptor and donor materials and depositing the bend on the substrate. On the contrary bulk inorganic photon absorption in organic semiconductor materials do not produce free charge carriers rather they generate strongly exciton which are known as tightly bound electron-hole pair [44]. However for optimum performance the distance between the exciton and the electron donor/acceptor interface should be within the same length range this explains why the bulk- heterojunction structure was introduced to enable the blending together of the donor electrons and acceptor materials [45].

It should be noted that another conducting layer is usually added between the anode and the photoactive layer as shown in figure 1. 9. This layer could serve as hole transporting layer (HTL) and exciton blocker. It also smoothens the indium tin oxide surface helps to seal the active layer from oxygen and also helps to prevent the diffusion of cathode materials into the active layers thereby enhancing the device stability [46]. If the diffusion was to occur it could lead to unwanted trap sites [40].

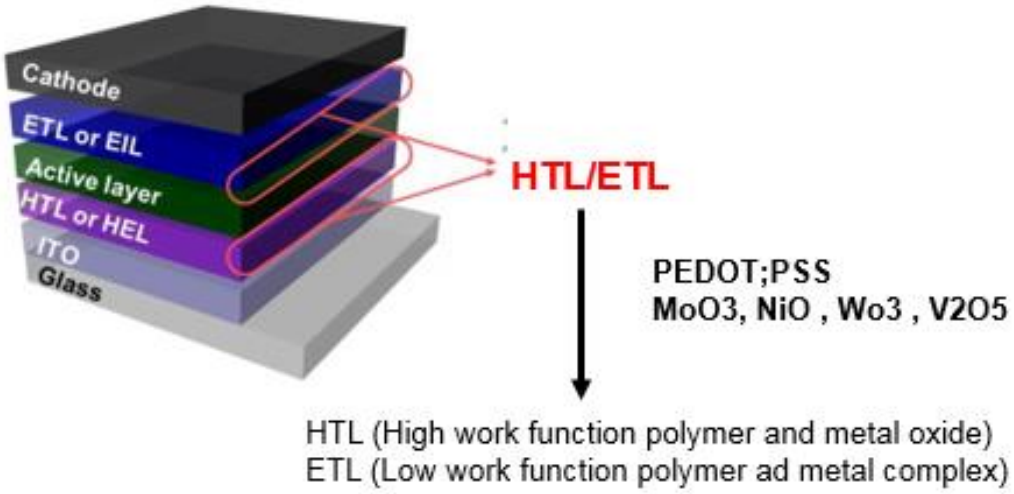

Figure 1. 8: Structure of an organic- inorganic hybrid solar cell.

PEDOT:PSS is the commonly used HTL because of its high work function , good electrical conductivity and the ability to reduce the surface of the surface roughness of indium tin oxide [47]. However, PEDOT: PSS is known to exhibit several problems which includes; inhomogeneous electrical properties which

often leads to weak long-term stability, highly hydrophilic with bad morphology. On the contrary transition metal oxides such as, V_2O_5, NiO, MoO_3 has been employed as HTL for hybrid solar cells by a plethora of researchers [48–50]. The metal oxides have been used as alternatives to PEDOT:PSS due to their high stability as visible in organic solar cell and flexibility in deposition method as they can be deposited using various methods such as electrodeposition, sputtering or vacuum evaporation [51,52]. Compared to other metal oxides MoO_3 has emerged as the promising alternatives to PEDOT: PSS as HTL because of its non-toxicity and non-corrosive nature together with its deep-lying electronic states [53]

1.3 Structure of MoO_3 thin films

Molybdenum oxide has been a subject of immense interest due to their unique electrical and optical properties, it is widely perceived that the transition metal oxide can be switched between two different optical states due to its thermochromic, photochromic or electrochromic effect [54]. Thermochromic effect of films refers to the change in the optical properties of a substance with temperature. A film with thermochromic effect changes their optical properties reversibly when heated and reverts back to its original properties when the temperature is cooled to its initial temperature [55]. Photochromic as the name suggests refers to the reversible absorption changes the films undergoes when exposed to different types of irradiation and then retains its original properties without the irradiation while electrochromic effect is the ability of thin films to change their color due to an applied potential and returns back to its original form when the electric potential is reversed [55] . For Molybdenum oxide the MoO_{3-x} with oxygen deficient usually contains excess metal atoms. These metal atoms behave like doping centers that controls the electrical and optical properties of the films. α-MoO_3 exists with a layered structure with dual layers of MoO_6 octahedral that are joined together in the (1 0 0) and (0 0 1) directions by covalent bonds and (0 1 0) direction by weak Vander waals forces of attractions [54]. Due to the uniqueness of the Molybdenum oxides it finds useful applications in rechargeable micro batteries, optical switching, electrochromic materials and humidity sensors [56].

XRD patterns of MoO_3 films has been used to identify and study the phases present by a plethora of researchers [28,54,56]. XRD study of MoO_3 thin films by Mahajan et al., [28] showed that the deposited thin films are polycrystalline with well-defined diffraction peaks along (0 2k 0) reflections with k= 1, 2 and 3 (Figure 1. 10). Their results also show that the films contain MoO_3 with α-orthorhombic structure. One important observation is the increase in crystallinity with solution concentration, however the authors attributed this to the increment in crystal size as the concentration increases [28]. A similar study by Boudauord et al., [56] also confirm the polycrystalline structure of MoO_3 films.

1.3.1 The role of MoO_3 in the interface of the hole conductor/cathode electrode

The use of MoO_3 as interfacial material in hybrid solar cell is very critical to the performance and stability of the solar cell. MoO_3 helps in the optimization of the electric contacts between the electrodes and the active layers leading to improved charge transfer and collection [27]. In bulk heterojunction solar cells (BHJ) a bicontinuous pathway is created for charge carriers to migrate to their corresponding electrode. However, it should be noted that in the active layer of the BHJ, both the donor and acceptor semiconductor are randomly distributed. The donor is usually a polymer most often poly (3-hexylthiophene-2,5-diyl) (P3HT) while the acceptor is a fullerene derivative usually phenyl-fullerene-butyric acid methyl ester (PCBM). There is a possibility that both the donor semiconductor and acceptor semiconductor could be in intimate contact with the cathode and anode in the solar cell. Recombination of charge carriers at the electrode would greatly reduce the PCE and stability of the solar cell. For this reason, interfacial materials such as MoO_3 is introduced to ensure that charge carrier recombination is greatly reduced by allowing the movement of the preferred charge carriers and blocking the movement of unwanted charge carriers. With the use of interfacial materials, the PCE of solar cells is greatly improved [27,57–59] .

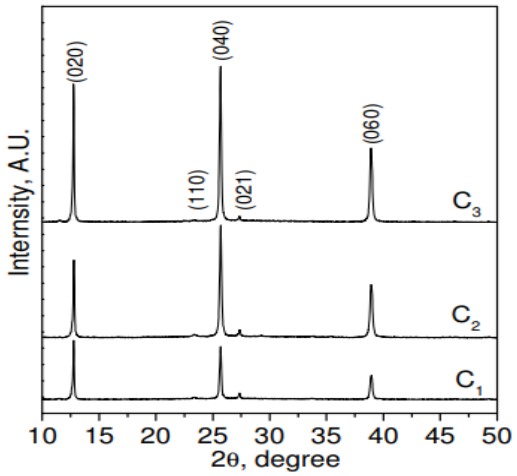

Figure 1. 9: XRD patterns of MoO_3 thin films deposited by spray pyrolysis at different solution concentrations 5 mM (Mo1), 10 mM (Mo2) and 15 mM (Mo3) at 350°C substrate temperature [adapted from ref. [28]].

As shown in figure 1.11 interfacial materials could be HTL or ETL. The diagram illustrates the schematics representation of conventional hybrid solar cell and inverted solar cells with HTL and ETL. Figure 1.12 illustrates the energy level of a solar cell with MoO_3 as HTL.

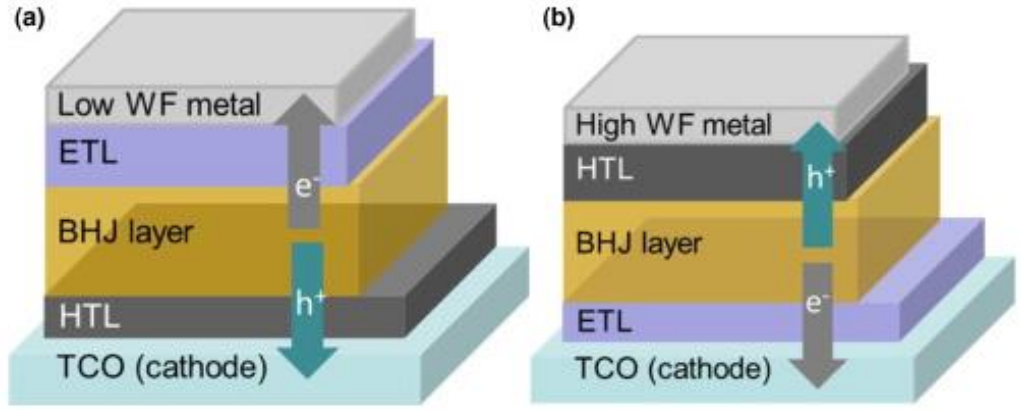

Figure 1. 10: Schematic representation of (a) conventional solar cell and (b) inverted solar cell. [Adapted from Ref. [57]].

In an inverted solar cell, the polarity of the electrode material collecting the charge is reversed. When compared to the conventional solar cell configuration, the inverted structure is suitable for large scale roll to roll processing. Furthermore, the use of high work function metal electrodes provides superior device stability.

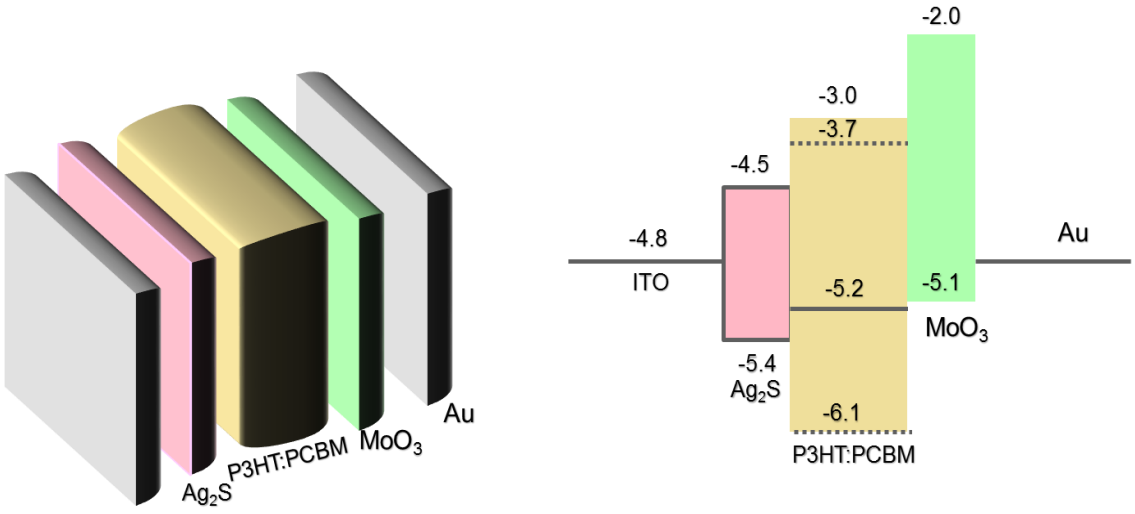

Figure 1. 11: Energy diagram of a solar cell with configuration of ITO/Ag_2S/P3HT: PCBM/MoO_3/Au.

1.4 Method of MoO_3 Deposition

A number of different methods could be used to prepare Molybdenum oxide thin films. Examples of such methods includes, chemical bath deposition, spray pyrolysis, electrodeposition, sputtering and thermal evaporation. The next section would discuss each of the methods.

1.4.1 Chemical bath deposition

Chemical bath deposition methods also known as controlled deposition, solution growth or simply chemical deposition method is relatively inexpensive, flexible and easy for large surface area deposition and does not require the use of sophisticated instruments such as a vacuum system [60]. Instead it uses cheap and readily available materials such as hotplate with magnetic stirrers. Also, the required starting chemicals are inexpensive and available. It is similar in the liquid phase to the common chemical vapor deposition which occurs in the gaseous phase. Figure 1. 13 shows a schematic of the experimental set up for chemical bath deposition.

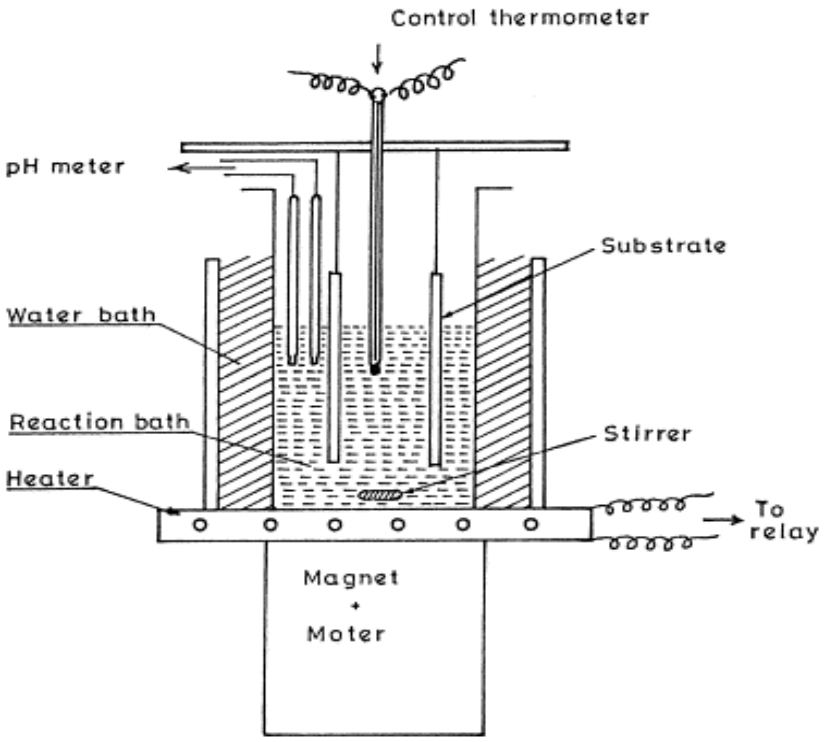

Figure 1. 12: Chemical bath deposition experimental set up system [adapted from ref. [60]].

As shown in the figure 1.13, the substrate and the films are placed stationary in the solution. With the aid of a magnetic stirrer the solution is stirred, and the chemical bath is heated to the desired temperature using paraffin bath or water. It should be noted that the stirring could be continuous from room temperature or it could be started only after attaining the required temperature.

1.4.2 Chemical Spray pyrolysis

Chemical spray pyrolysis has been used over the last decade for the deposition of a varieties of materials as thin films. This technique provides one of the most attractive way for the deposition of thin films of metal oxides, superconducting compounds, noble metals and chalcogenides [61]. Spray pyrolysis method offers the following advantages compared to other deposition methods: (i) its simplicity because it provides an easy way to dope films of any element and in any proportion by simply adding it in the form of a spray solution (ii) Unlike the Vapor deposition methods, spray pyrolysis techniques does not require a vacuum. This is an immense advantage especially when the process is required to be scaled up for industrial applications, also spray pyrolysis does not require substrates and/or high quality targets [61] (iii) The ability to control the thickness and deposition rate of the thin films by simply changing the spray parameters in this way some limitations of chemical methods such as films of limited thickness can be avoided (iv) This method does not produce any additional overheating that could destroy the materials unlike high powered methods like magnetic sputtering (v) Layered films with composition gradients can be obtained by simply changing the composition of the spray solution during the spray process. Figure 1. 14 illustrates a typical spray pyrolysis set up. The apparatus consists of a spray nozzle, substrate heater, temperature controller, precursor solution and gas propellant. Liquid and gas flow meters are often used to measure the flow of precursor's solution and the air. The spray pyrolysis set up is usually mounted on a moving table. It should be noted that properties of the produced films are largely dependent on the carrier gas, ambient temperature, droplet size, and the cooling rate after deposition. On the other hand, the film formation is dependent on the reaction, solvent evaporation and the process of droplet landing. Patil, [45] presents an excellent review of chemical spray pyrolysis technique.

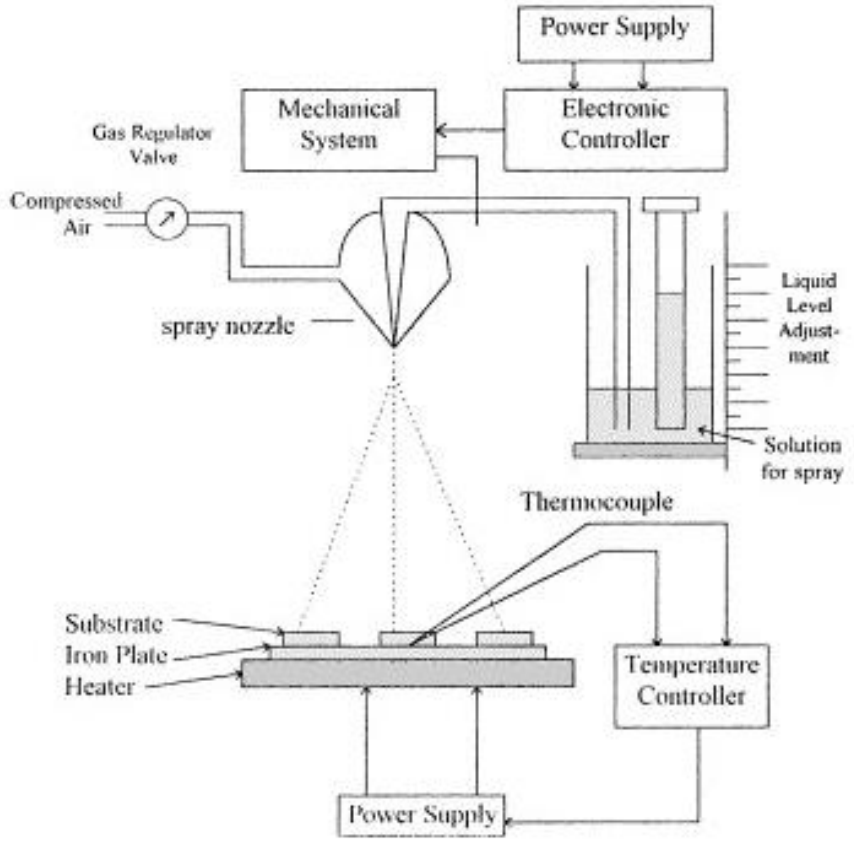

Figure 1. 13: Experimental set up for spray pyrolysis system [adapted from [61]].

1.4.3 Electrodeposition

Electrodeposition is widely regarded as an environmental friendly deposition technique that does not need vacuum environment or high temperature treatment to produce a solar cell [62]. The technique is good and highly efficient when film thickness and surface profile of the deposited film is to be varied [63]. During electrodeposition, materials wastage can be greatly minimized by controlling the deposition parameters. Analogous to vacuum thermal evaporation, electrodeposition allows the production of different layers of solar cells.

The schematics of a typical electrodeposition process is shown in figure 1.12.

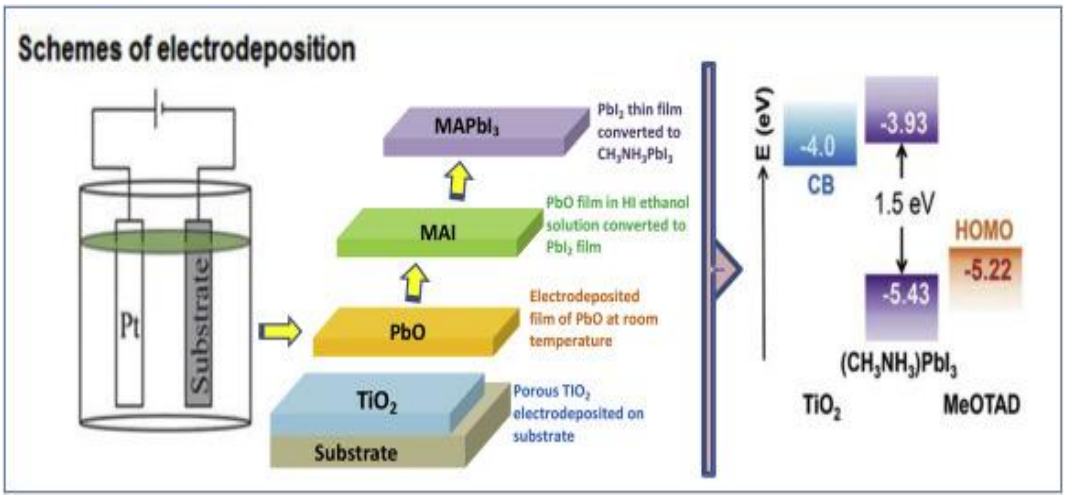

Figure 1. 14: Schematics of a typical electrodeposition process. in this process a perovskite $CH_3NH_3PbI_3$ formation onto compact TiO_2 on FTO substrate by the electrodeposition of PbO to initiate in-situ reaction to form perovskite layer [adapted from ref. [63]].

As shown in figure 1.15, electrodeposition the electrochemical reaction starts with PbO which then diffuses into the surface of the electrode (the substrate coated with TiO_2) to form a perovskite thin layer. The uniqueness of this process lies in the ability to produce a uniform thin film by easily controlling the thermodynamic deposition parameters which are directly related to the specific film thickness and smooth surface profile enhancements [62]. It should be noted that uniformly deposited thin films enables the increase in power conversion efficiencies in devices by controlling the deposition time, concentration of the electrolytic solution and the deposits [64].

1.4.4 Vacuum thermal evaporation

In vacuum thermal deposition the substance from the thermal vaporization sources reaches the substrate without collisions or limited collision with the gas molecules in the space between the substrate and the source. The vaporized material is always placed in a manner that it aligns with the sight of the source. The vacuum environment is designed in such a way that it provides the capacity to minimize gaseous contaminants in the deposition system to the lowest level [65]. A gas pressure range of 10^{-5} Torr to 10^{-9} Torr is usually required for vacuum evaporation depending on the nature and quantity of gaseous material in the system. Compared to other deposition methods vacuum thermal evaporation produces a uniform microstructure and requires low process temperature on the substrate. In this work vacuum thermal deposition was used as the deposition technique.

1.5 The Scope of the present work

Based on literature review it is evident that hybrid solar cells with inverted configuration have immense advantages and would be beneficial in the photovoltaic industry to replace the expensive solar cells made from silicon materials. However, their low efficiency and life span is still a critical issue that needs further attention. This necessitated the use of interfacial buffer layers. Molybdenum oxide is identified as a very important protective for hybrid solar cells due to their wide range of band gap, ability to exist in different valence states and layered structure. In order to use MoO_3 as a buffer layer for hybrid solar cells it is important to optimize the growth conditions and produce pure thin films with precise morphology, structure and optical properties. A profound understanding of the composition, structure and properties of MoO_3 thin films is invaluable for the optimization of the growth conditions.

The present research focus on using Vacuum evaporation method to prepare MoO_3 thin films on glass substrate and investigation of the structural and optical properties of the films. Furthermore, the effect of post deposition temperature on structural and optical properties of MoO_3 thin film is studied. The novelty of the work lies in the fact that no study has attempted to investigate the structural and optical properties of MoO_3 as an interfacial buffer layer for an inverted hybrid solar cell using vacuum evaporation method. Finally, the prepared MoO_3 film was tested as a buffer layer in hybrid solar cell ITO/TiO_2/Sb_2S_3/P3HT/MoO_3/Au and the J-V measurement is compared with that of a reference ITO/TiO_2/Sb_2S_3/P3HT/ Au solar cell.

1.6 The Aim of study

The overall aim of the present thesis is to understand the structural and optical properties of vacuum deposition MoO_3 thin films which is to be used as an interfacial buffer layer for hybrid solar cells. This is achieved sequentially as thus;

- To deposit MoO_3 on glass substrate using vacuum thermal evaporation method.
- To analyze the structural properties of the produced thin films (XRD, SEM, EDX), and the optical properties (transmittance, reflectance and band gap).
- To heat MoO_3 thin films at different temperatures and investigate the effect of temperatures on structural and optical properties.
- To deposit MoO_3 on an inverted solar cell with configuration ITO/TiO_2/Sb_2S_3/P3HT/MoO_3/Au.
- Determine the performance of the hybrid solar cells ITO/TiO_2/Sb_2S_3/P3HT/MoO_3/Au against a reference solar cell ITO/TiO_2/Sb_2S_3/P3HT/ Au.

CHAPTER II: EXPERIMENTAL METHODOLOGY

2.1 Preparation of MoO_3 thin films

MoO_3 thin films were deposited on a glass surface by vacuum thermal evaporation method as shown in Figure 2.1. MoO_3 powder was used as the evaporation material which was deposited on a glass substrate. MoO_3 powder was purchased from Alfa Aesar with 99.5 % purity. The samples of MoO_3 were heated in a vacuum evaporator and then evaporated using Molybdenum (Mo) boat at 19 Amperes from 2 seconds to 10 minutes depending on the thickness of the glass. The quartz crystal control monitor was used to control the thickness of the film produced and the rate of deposition. After the deposition process all films produced were thermal annealed in air for 30 minutes at temperatures of 150, 200, 300, 400 and 500 ^oC. This procedure is important in order to study the effecting of temperature on the structure and properties of the films produced.

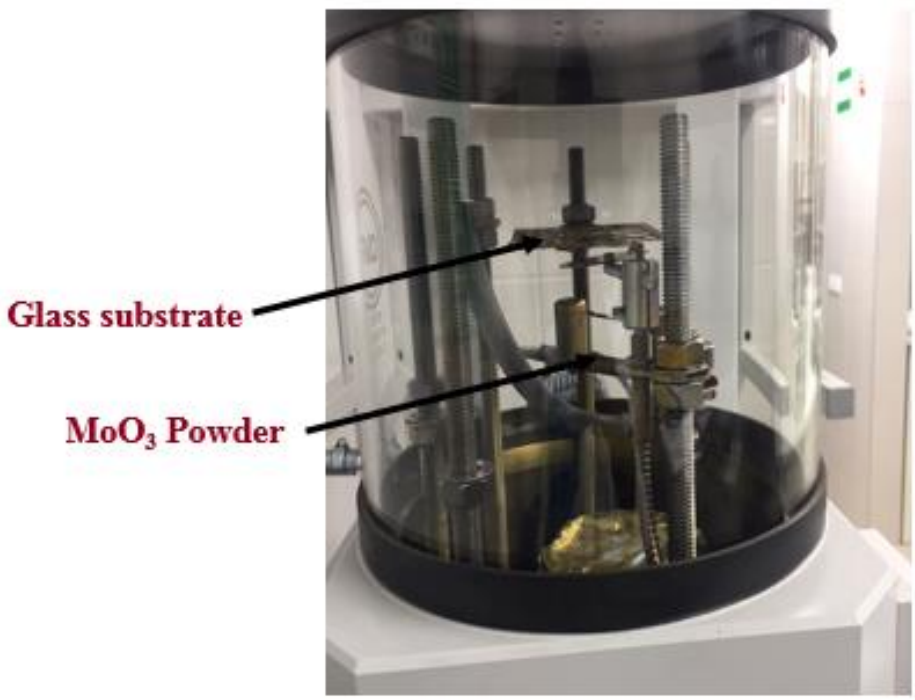

Figure 2.1: Vacuum thermal evaporation of method to produce MoO_3 thin films.

2.2 Characterization of MoO_3 thin films produced

MoO_3 thin films produced were characterized by Optical transmittance (UV-VIS), scanning electron microscopy (SEM), X-ray diffraction (XRD) methods and energy dispersive X-ray spectroscopy (EDX).

2.2.2 Ultraviolet–visible spectrophotometry

To determine the optical absorption coefficient and energy band gap the optical measurement of MoO_3 thin films was carried out using a using a Jasco V-670 UV-VIS-NIR spectrophotometer (Jasco Corporation, Ishikawa-cho, Hachioji-shi, Tokyo, Japan) in the range of 250-1200 nm. UV-Vis spectrophotometry refers to the absorbance or transmittance spectrophotometry in the visible light region and it works on the principle that the absorption of energy from the incident light allows electrons to be excited from lower energy state to a higher energy state.

2.2.3 Scanning electron microscopy (SEM)

SEM images of MoO_3 thin films were observed using EVO MA 15 Zeiss apparatus (Carl Zeiss, Inc., Oberkochen, Germany). SEM images helps to evaluate the thickness as well as the morphology of MoO_3 thin films. SEM images of the thin films are taking by focusing the samples on the election beam where the electrons are made to relate with the atoms in the sample. In that way signals that contains information relating to the surface morphology and composition of the samples will be produced. Figure 2.2 represent schematic diagram of SEM.

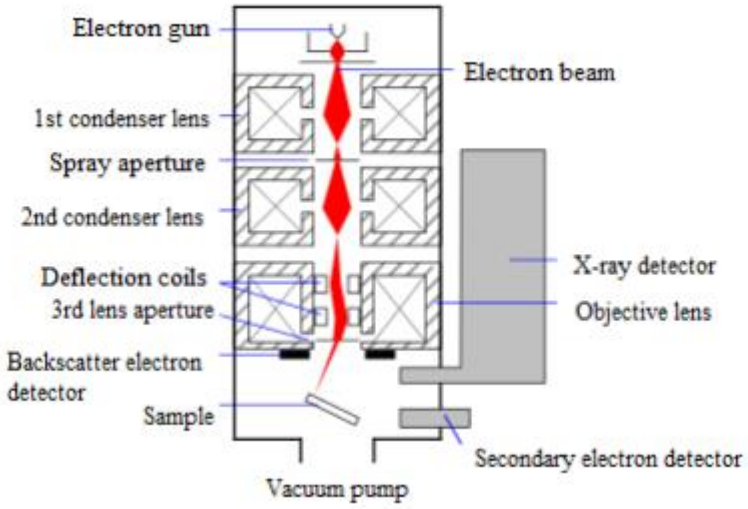

Figure 2.2: Schematics diagram of SEM.

SEM is a kind of electron microscopy that takes images of a samples by scanning it with high energy beam of electrons. The electrons are made to interact with the atoms present in the samples thereby producing signals that contains the surface topography and morphology of the materials. The apparatus consists of the electron gun unit, scanning unit, demagnification unit, focus unit and detector unit. The electron gun produces a beam of scattered electrons which is narrowed down by the condenser lens in the demagnification unit. The produced electron is focused on the sample with the aid of an electromagnetic lens in the focusing unit which then scans the sample.

2.2.4 X-ray diffraction (XRD) and Energy dispersive X-ray analysis (EDX) Analysis

XRD patterns of MoO_3 thin films were recorded using a Rigaku Ultima IV diffractometer (Rigaku, Shibuya-ku, Tokyo, Japan) with Cu Kα radiation, λ = 1.5406 Å, 40 kV at 40 mA in the 2ϑ range of 20° - 80°. XRD technique is used to determine the presence of atomic and molecular structure of crystals. The atoms cause a beam of x-rays to diffract into different directions. XRD works on the principles of X-ray diffraction in which an incoming beam of light which is directed towards a crystal is scattered as they pass through atoms of the crystals. The scattered rays relate with each other and generates spots with different intensities that can be recorded on the film.

EDX analysis of MoO_3 thin films was carried out using a Zeiss HR FESEM Ultra 55 with Bruker EDS system. The EDX set up consists of an X-ray detector, pulse processor, the exciton source which is usually the X-ray beam and the analyzer. EDX is often used for the chemical characterization and elemental analysis of a sample. It works by depending on the collaborations between the sample and the source of X-ray. IN this study we use EDX to determine the elemental composition of the produced MoO_3 thin films.

2.3 Determination of the output parameters of the Hybrid solar cells.

To ascertain the performance of the prepared MoO_3 thin film on hybrid solar cells J-V curve measurements of the hybrid solar cells was carried out. The MoO_3 film was vacuum deposited on the cleaned ITO/TiO_2/Sb_2S_3/P3HT structure. It should be noted that the already stacked structure of ITO/TiO_2/Sb_2S_3/P3HT was prepared by another researcher in our laboratory. The preparation of this structure is not within the scope of the current study. This study only aims to ascertain the performance of MoO_3 as interfacial layer in the structure. Then gold (Au) which serves as the cathode material was deposited on the active layer through thermal evaporation method. The J-V characteristics of solar cell ITO/TiO_2/Sb_2S_3/P3HT/MoO_3/Au was measured and compared against a reference solar cell without MoO_3.

Figure 2.3 shows a schematics arrangement of the inverted solar cell and the reference solar cell.

Reference

ITO/TiO_2/Sb_2S_3/P3HT/Au

(Indium tin oxide/ Titanium dioxide/ Antimony trisulfide/ poly (3-hexylthiophene-2,5-diyl) /gold)

Inverted solar cell

ITO/TiO_2/Sb_2S_3/P3HT/MoO_3/Au

(Indium tin oxide/ Titanium dioxide/ Antimony trisulfide/ poly (3-hexylthiophene-2,5-diyl) /Molybdenum trioxide/gold)

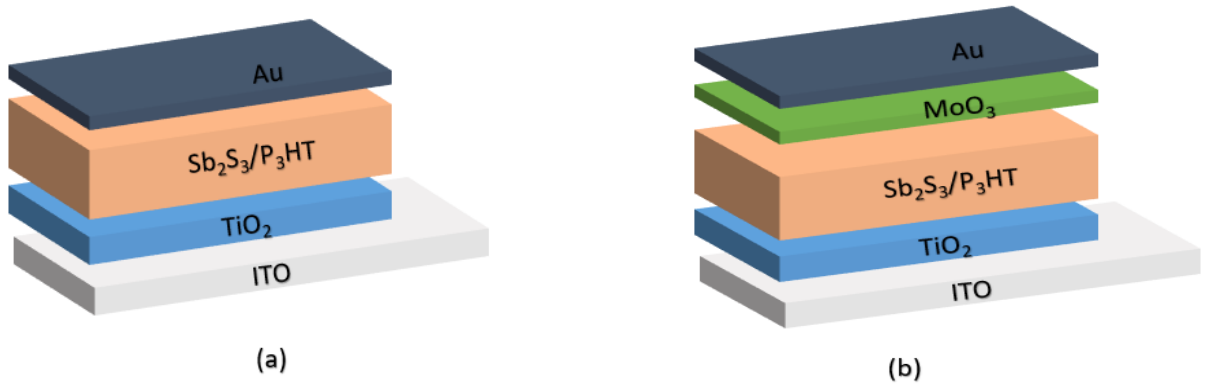

Figure 2.3: Schematics of the hybrid solar cell used in this study and the reference solar cell. (a) ITO/TiO_2/Sb_2S_3/P3HT/Au and (b) ITO/TiO_2/Sb_2S_3/P3HT/MoO_3/Au.

CHAPTER III: ANALYSIS OF RESULTS AND DISCUSSION

3.1 Physical appearance of MoO_3 thin films after post deposition thermal annealing

The deposited thin films were heated in air at temperatures of 150, 200, 300, 400 and 500 ^oC. The resulting MoO_3 thin film after thermal treatment are represented by M1, M2, M3, M4, M5 and M6. The as - deposited thin film is denoted by M1, while M2 to M6 represents films annealed at temperatures of 150, 200, 300, 400 and 500 ^oC respectively. Figure 3. 1 shows the appearance of specimens after thermal treatment in air. At different temperatures of the samples there is a variation in transparency. The as deposited MoO_3 samples is identified with a blue color. The blue coloration might be because the film is not prepared in the dark rather through Vacuum thermal evaporation. Due to the Vacuum, Mo atom could possibly change its valence state from 6+ to 5+ [as well as to 4+ (MoO_2) if the amorphous film is continuously heated in the Vacuum [66]. Electrons are transferred from valence 2p oxygen orbitals to empty Mo^{6+} (4d) level which gives rise to an incorporation of lower valence Mo^{5+}within the lattice. The color darkens to deep blue after thermal annealing up to 200 °C. This shows that the post deposition heating of MoO_3 samples produces free electrons which form color centers when trapped by ion vacancies [67]. Above thermal annealing temperature 200 °C there is an increase in the transparency of MoO_3 thin films, which clearly highlights the non-linear dependency of the transparency of MoO_3 thin films with temperature when heated in air. On the contrary, a similar study by Lin et al., [68] where the authors prepared MoO_3 thin films by electron beam evaporation and carried out their post annealing in Nitrogen they noticed a linear dependency of the transparency of the of MoO_3 thin films with temperature. The appearance of their specimen after annealed at different temperatures in N_2 is shown in figure 3.2. We envisage that the differences between our findings and theirs might be because of the disparity in deposition and heating methods. Those two parameters could have effect on the transparency of the thin films produced. To validate the hypothesis the physical appearance of the films obtained from our study is compared to that of Sian and Reddy [69] who used a similar vacuum thermal deposition method and thermal annealing in air. It is no surprise that the two results were identical. They also obtain a light blue as deposited thin films, the color becomes darker after thermal annealing in air for an hour. As they increased the annealing temperature above 350 °C the produced films becomes lighter which indicates a non- linear dependency of transparency with annealing temperature.

3.2 Optical Properties of MoO_3 films and band gap measurements

Figure 3.3 depicts the optical transmittance spectra of spectra of MoO_3 films annealed at various temperatures with wavelength ranging from 250-1200 nm. The MoO_3 thin film samples shows a wide variation in transmittance at different thermal annealing temperatures. Starting with the as- deposited samples, as the temperature increases to 150 °C and to 200 °C, the total transmittance declines in the same order. However, a surge in the total transmittance was observed when the MoO_3 thin film samples are annealed at temperatures above 200 °C. A rise in temperature from 300 – 500 °C brings about a subsequent increase in the total transmittance. The change in the transmittance of MoO_3 thin films at different annealing temperature could be because of its thermochromic effect. As explained in the previous section, thermochromic properties refers to the reversible change in the optical properties of a substance with temperatures. In terms of increasing total transmittance the thin films could be arranged in the order of M3<M2<M1<M4<M5<M6 with M6 exhibiting the highest total transmittance of about 85% and M3 having the lowest total transmittance of about 20%. One interesting observation is the correlation between the intensity of the blue coloration and the transmittance of MoO_3 samples. MoO_3 samples annealed at 200 °C (M3) has the lowest transmittance and the deepest blue coloration. We presumed that the variation in transmittance and the color change of molybdenum oxide annealed at various temperature is due to the photochromic and thermochromic effects of the material [70]. The unique feature distinguishes MoO_3 as a very interesting metal oxide with great potentials for diverse engineering applications. Analogous to this study, Lin et al., [68] also observed this interesting observation. In their findings there is a correlation between the total transmittance of the MoO_3 thin film samples annealed at various temperatures and the transparency of the films. The results from our study shows that both the transparency of the MoO_3 thin films and their total transmittance exhibits a non – linear relationship when thermal annealed in air. In another study by Boukhachem et al.[71] the authors prepared MoO_3 thin films by spray pyrolysis, they obtained a maximum total transmittance of about 45% for the as-deposited MoO_3. As stated earlier, the disparity in total transmittance could be attributed to different deposition methods used.

The absorption coefficient and the optical band gap values were determined from the total transmittance data. The absorption coefficient (α) was calculated using the expression:

$$I = I_o e^{-\alpha d}, \qquad [1]$$

Where I_0 and I are the intensities of the incident and transmitted radiation, respectively, and d is the thickness of the film. The band gap of MoO_3 films were calculated by using the expression [72]:

$$\alpha h\nu = A\left(h\nu - E_g\right)^{\frac{1}{n}}, \qquad [2]$$

Where α is the absorption coefficient, A is a constant related to the effective masses of charge carriers, h is the Planck constant, E_g is the band gap energy, hv is the incident photon energy, and 1/n is the exponent that depends on the nature of the optical transition (n = 0.5 and 2 for direct and indirect transition, respectively). For the direct band gap estimation, a plot of $(\alpha h\nu)^2$ against the photon energy is used to estimate the band gap.

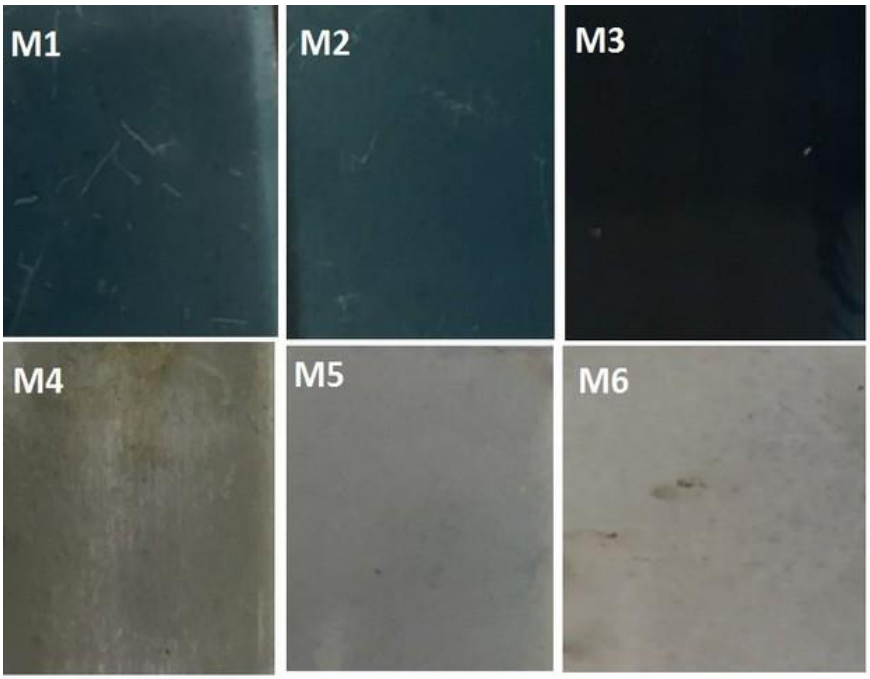

Figure 3.1: Appearance of different specimen after thermal annealing in air at different temperatures (M1 as deposited, M2 – M6 represents annealing temperatures of 150, 200, 300, 400 and 500 ^{o}C respectively. The thin film was produced by vacuum thermal evaporation.

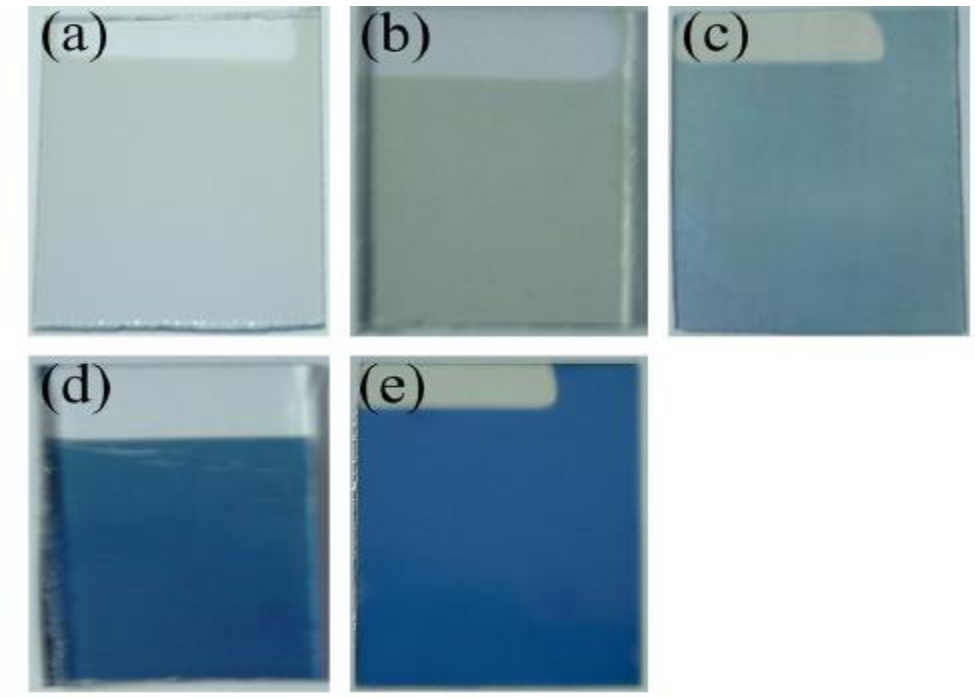

Figure 3.2: Appearance of different specimen after thermal annealing in Nitrogen at different temperatures. (a) as-deposited; (b) 200 °C; (c) 300 °C; (d) 400 °C; (e) 500 °C. The thin film was produced by electron beam evaporation [adapted from ref [68]].

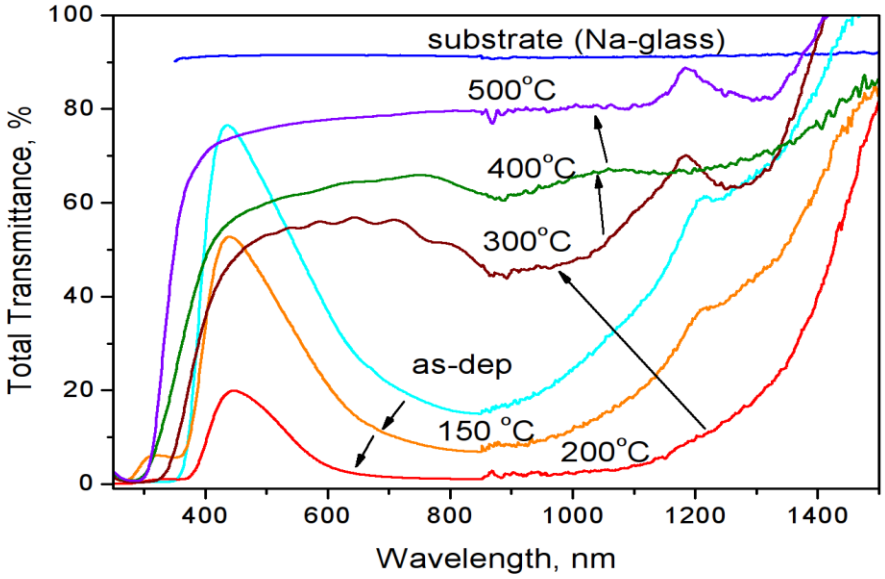

Figure 3.3: Total Transmittance spectra of MoO_3 films annealed at various temperatures in air. Thin films produced by vacuum thermal evaporation.

Band gap of MoO_3 films were estimated by fitting the linear region of the plot to the zero axis. Figure 3.4 represents the plot of $(\alpha h\nu)^2$ versus energy of photon for as-deposited films. The band gap estimated from the plot is 3.3 eV. Our optical band gap value for the as-deposited MoO_3 thin films is consistent with literature values. Boukhachem et al.[71] obtained an optical band gap of 3.46 eV for MoO_3 thin films produced by spray pyrolysis. Lin et al., [68] produced MoO_3 thin films with electron beam evaporation and obtained an optical band gap of 3.96 eV. Since the band gap calculated is more than 2.4 eV, MoO_3 is considered a wide band gap semiconductor.

To investigate the relationship between the optical band gap (E_g) and thermal annealing temperature, we calculated E_g values for all the MoO_3 thin film samples annealed at various temperatures. Results of the calculations is presented in Table 3.1. The plots used to estimate Eg values are displayed in Appendix A1. The band gap is within the range of 3.1 – 3.86 eV for thermal annealing temperatures of 150 – 500°C. The variation in optical band gap further elucidates the hypothesis that MoO_3 is a wide band gap semiconductor.

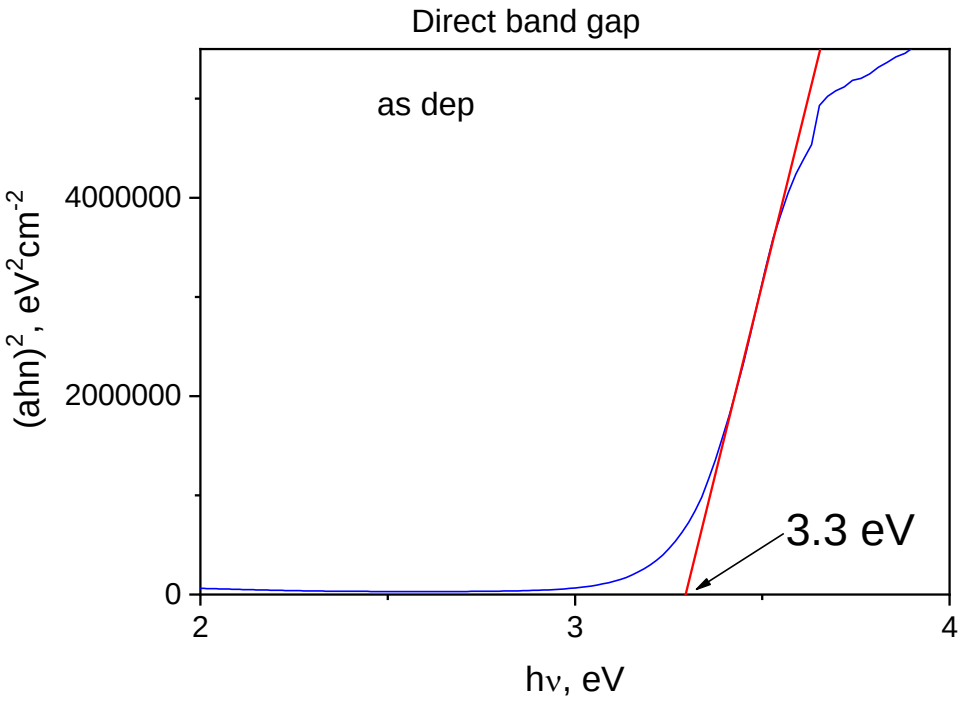

Figure 3.4: Plot of $(\alpha h\nu)^2$ versus energy of photon for as-deposited films.

The Eg value of MoO_3 films heated at 150 °C is 3.1 eV, the value decreases to 2.8 eV when the sample is heated up to 200 °C. Subsequently as the temperature increases from 300, 400 and 500 °C, Eg values rose to 3.49, 3.78 and 3.86 eV respectively. The drop in Eg as the temperature rises to 200 °C could be as a result of the formation of additional oxygen vacancies in the films. Lin et al., [73] suggested that the vacancies are generated during the deposition and thermal treatment of MoO_3 films. These oxygen vacancies produces extra energy level in the energy gap which are relatively close enough to the valence band to act as donor centers and reduce the energy gap [69]. Therefore, as thermal treatment temperature increases up to 200 °C there is a proliferation in the concentration of oxygen vacancies leading to a reduction in the Eg of the films. In contrast, the increase in Eg of the films with annealing temperature from 200 °C to 500 °C is due to the partial filling of oxygen vacancies. Ramana and Julien [74] proposes that the oxygen might be prevented from entering the growing lattice of the substrate if re-evaporation from the film surface occurs. The sudden rise in Eg as the thermal annealing temperature is increased to from 200 to 300 °C could be explained by considering the fact that longer annealing temperature would require extended heating time in air. This means that the films would be exposed to more oxygen than required thereby decreasing the concentration of oxygen vacancies. This also explains the increase in transparency of the films at temperatures above 300 °C.

Table 3. 1: The optical band gap (Eg) of as-deposited and after annealed at 150, 200, 300, 400 and 500 °C samples respectively.

Sample name	**Temperature (^{O}C)**	**Direct band gap Eg, (eV)**
M1	As deposited	3.3
M2	150	3.1
M3	200	2.8
M4	300	3.49
M5	400	3.78
M6	500	3.86

3.3 X-Ray Diffraction (XRD) Result Analysis

XRD patterns for the as-deposited MoO_3 films and MoO_3 films heated at various temperature in air are presented in figure 3.5a and 3.5b. The as-deposited MoO_3 films and films heated up to 200 °C are amorphous because no visible crystalline phase was observed in their XRD pattern. However, the crystallinity of the films increases with temperature above 200 °C. Consequently, the crystalline temperature of MoO_3 would probably be above 200 °C. At 500 °C, XRD shows well defined peaks of (020), (010), (040), (101), (060), (211), (171) and (261). At 300 °C the predominant peak is (040), (021) and the main crystalline phase is the α-MoO_3 phase. This is confirmed by the presence of peaks like (040) and (060). At about 400 °C XRD patterns detects the existence of two phases (α- $Mo0_3$ and Mo_5O_{14}), as the temperature increases to 500 °C only one phase is present which is (α-MoO_3). Hence it can be deduced that α-MoO_3 is thermally stable. Similar results was obtained by Lin et al., [73]. Their findings confirm that the as-deposited MoO_3 thin films were amorphous, and no crystalline phase was observed as the films are annealed in both air and N_2 at temperatures below 200 °C. Another study by Sian and Reddy [69] also displayed similar results. Their XRD results indicate that the as-deposited thin films and films annealed for temperatures up to 150 °C are amorphous. However, they suggested a temperature of 240^{0}C as the offset crystallization temperature of the films.

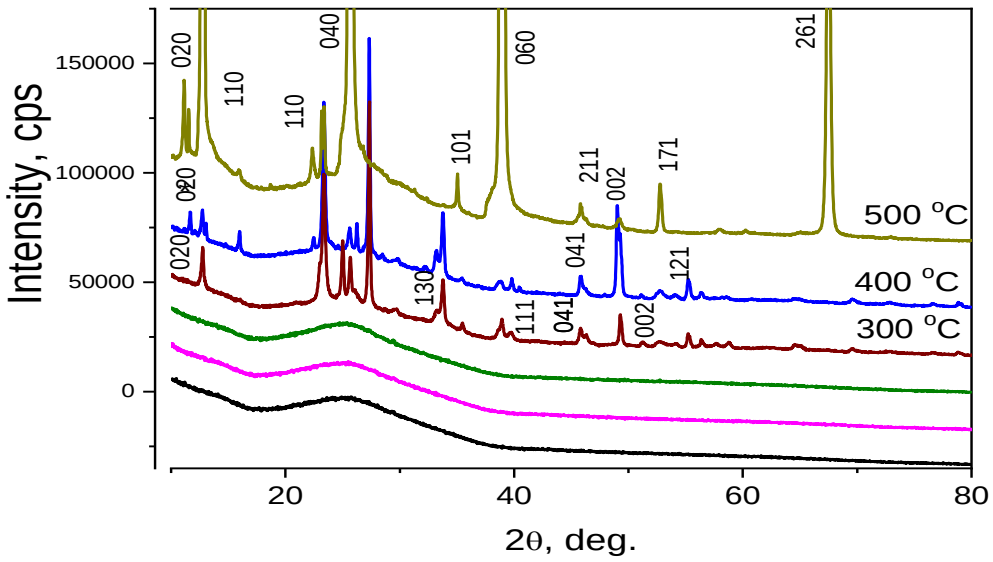

Figure 3.5a: XRD Patterns of MoO_3 films produced at various annealing temperatures in air.

.

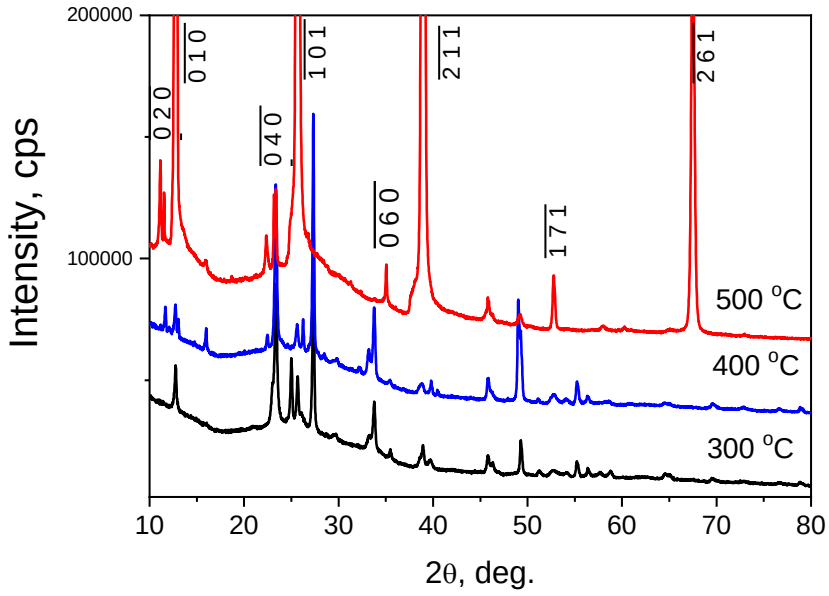

Figure 3.5b: XRD Patterns of MoO_3 films produced at various annealing temperatures in air showing their well-defined peaks.

Some structural calculations are carried out to obtain more information about the structural quality of the deposited MoO_3 samples.

Lattice parameters were calculated according to the following equations:

$$\frac{1}{d_{khl}^2} = \frac{h^2}{a^2} + \frac{l^2}{b^2} + \frac{l^2}{c^2} \qquad [3]$$

Where d_{khl} is the plane spacing values related to the Miller indices h,k and l and a,b and c are the lattice parameters [75,76]. The values of lattice parameters obtained in Table 3.2 ranges from 3.6 to 13.9 Å. The value is similar to the results of Boukhachem et al.,[71]. The values of the lattice parameters are close to that of α-MoO_3.

Dislocation density (δ) of a crystal measures the number of defects present in the crystal [77]. It is defined as the length of dislocation lines per unit volume. It can be estimated from the expression [75]:

$$(\delta) = \frac{1}{D^2} \qquad [4]$$

The value of dislocation density of different samples is expressed in the Table 3.2. The dislocation density decreases significantly from 277.8 $\cdot 10^{-14}$ lines/m^2 to 0.77 $\cdot 10^{-14}$ lines/m^2 as the annealing

temperature of the samples increases from 300 °C to 500 °C respectively. This could possibly mean an increase in the amount of defects present in each crystal as the temperature increases.

The Debye– Scherer formula was used to estimate the crystallite size. The expression is shown below [75,78]:

$$D = \frac{k\lambda}{B_{\frac{1}{2}} cos(\theta)} \quad [5]$$

Where k =0.90 is the Scherrer constant and λ=1.54 Å is the wavelength of CuKα radiation [75]. From the table above it shows that the crystallite size increases with temperature.

Table 2.2: Calculated values of the lattice parameters, crystallite size and dislocation density for MoO_3 thin films at various annealing temperatures.

Sample name	**Lattice parameters**			**Phase**	**Crystallite size (nm)**	**Dislocation density (δ) (10^{14} lines/m^2)**
	a (Å)	**b** (Å)	**c** (Å)			
M6	3.96	13.8	3.6	α-MoO_3	135.40	0.55
M5	3.95	13.9	3.7	α-MoO_3	32.30	9.59
				Mo_5O_{14}	32.60	9.39
M4	3.96	13.9	3.7	α-MoO_3	6.0	277.80
M3	**Amorphous**					
M2	**Amorphous**					
M1	**Amorphous**					

3.4 Energy dispersive X-ray spectroscopy (EDX) Analysis

Table 3.3 illustrates the EDX results of MoO_3 films and MoO_3 films annealed at various temperatures. According to the EDX results the films composed of molybdenum (Mo), oxygen (O), Silicon (Si) and Sodium (Na) with different compositions based on the annealing temperatures. We could deduce from the EDX results that thermal annealing changes the crystalline structure, but the chemical composition remains similar. Since the O/Mo ratio approximately 3 at all temperatures. It should be noted that the presence of Na and Si is due to the glass substrate used for MoO_3 deposition.

Table 3.3: EDX results for MoO_3 films annealed at various temperatures in air.

Na-glass / MoO_3

Vacuum evaporation

30 minutes thermal treatment

heat treatment, in air, °C		Mo, at%	O, at%	Si, at%	Na, at%	O/Mo ratio
–		24.2	74.7	0.8		3.0
150		26.6	71.7	1.2		2.6
200		25.0	72.9	0.5	1.2	2.9
300		25.8	72.4	0.2	1.3	2.8
400		20.7	67.5	8.5	3.3	2.4
500	1. cryst.	24.4	75.3			3.1
	2. rest.	35.5	47.2	2.7	13.9	1.0
	3. rest.	19.0	62.0	7.6	11.0	2.2

* In order to calculate the O/Mo atomic ratio we exclude the SiO_2 and Na_2O from the equation.

3.5 Scanning electron microscopy (SEM) Results

SEM microscopy of MoO_3 films and MoO_3 films annealed at various temperatures was performed to reveal the surface and the thickness of the films. The as-deposited films have smaller and fine grains compared to the films annealed at various temperatures. As the temperature increases to 150 °C the films exhibits a much finer grains having smaller thickness. The visual appearance of as- deposited films and films annealed at 150 °C confirms their amorphous nature. At thermal annealing temperature of 200 °C large particle grains begins to form. MoO_3 films annealed at 200 °C exhibits granular crystalline structures with lattice sites observed in the structure. On the contrary, blisters are observed on the surface of MoO_3 films formed at 300 °C. This could be as a result of the complete dehydration of the films. The grain size also increases with temperature while porous surface are visible [79]**.** Defects were observed in the SEM images at 300 °C. Formation of defects on the SEM images of MoO_3 films annealed at 300 °C is in agreement with the XRD results. Moreover, grains similar to Nanorods and paralleled to the substrate was formed when MoO_3 films was heated to 500 °C.

One important observation is the relationship between the film thickness and annealing temperature. With increasing annealing temperature, the films thickness decreases progressively as shown in Table 3.4. As MoO_3 films were heated from a temperature of 150 °C to 200 °C, there is a reduction in film thickness from 1348 nm to 1254 nm. Also, 62% decrease in film thickness was observed when MoO_3 films were heated up to 500 °C. Decrease in film thickness with temperature could be attributed to the coalescence of particles in the film structure, which led to the formation of large particle aggregates and scattered the light [80] thereby increasing its transparency**.**

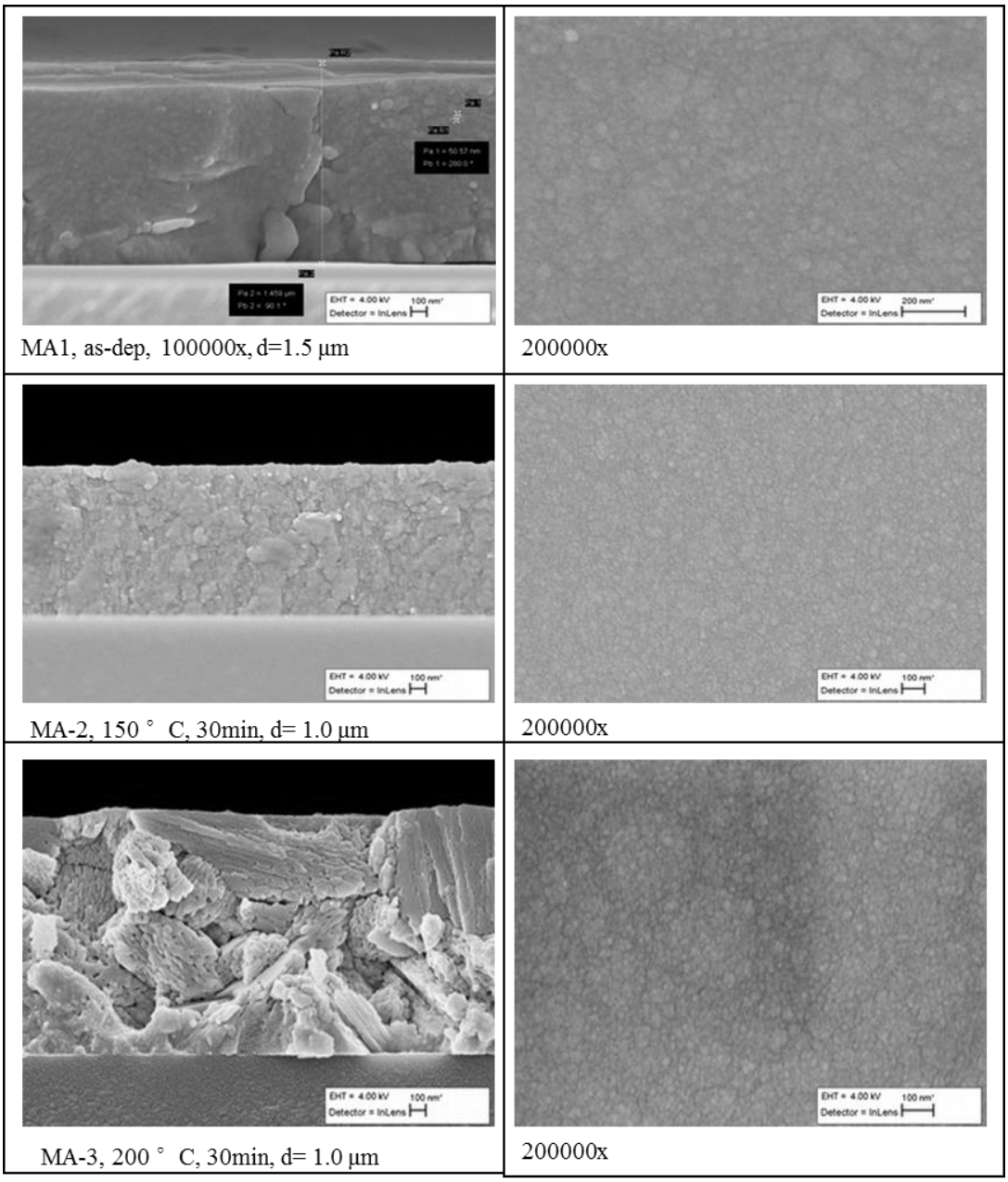

Figure 3.7: SEM images of M1 -M3 samples.

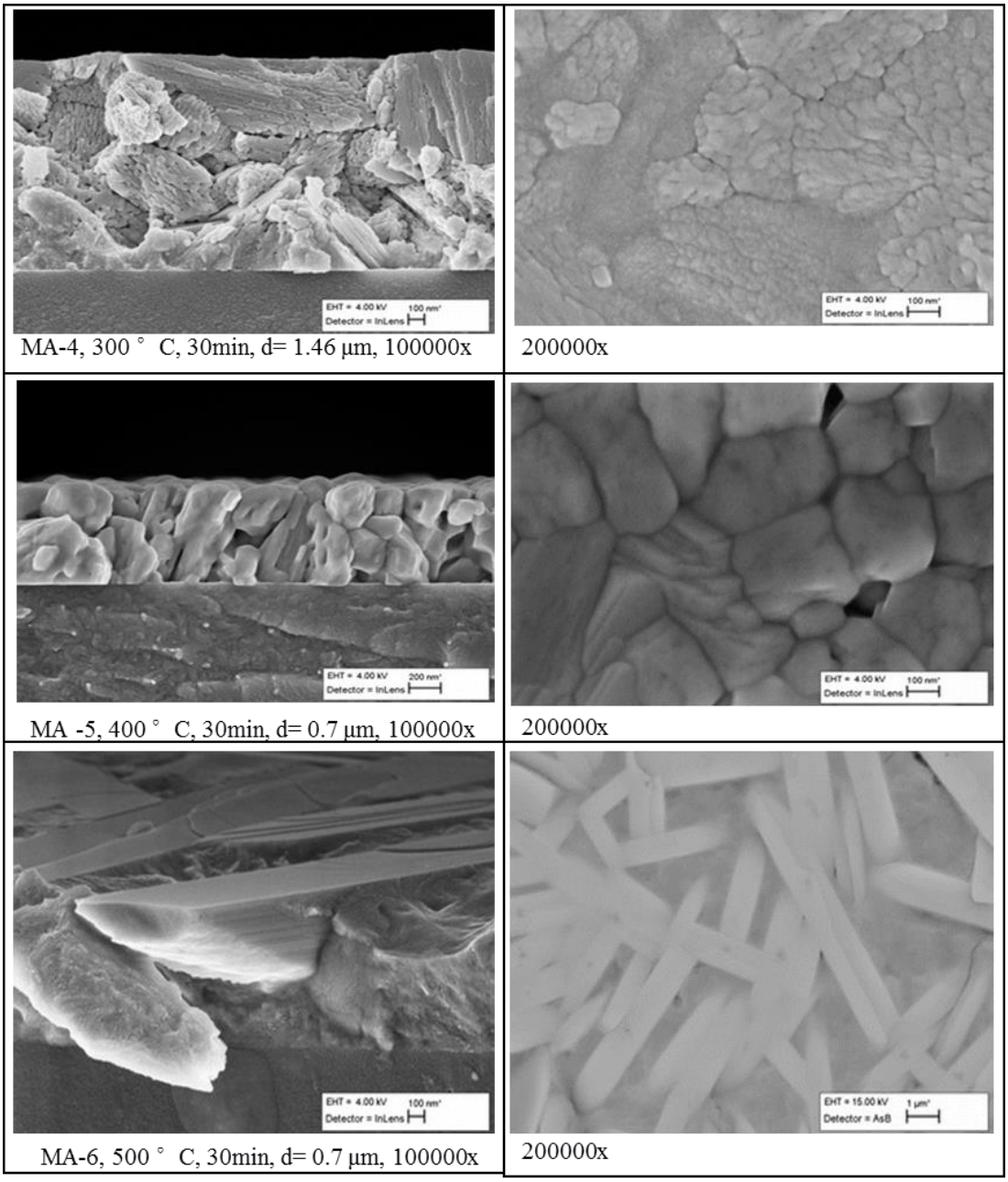

Figure 3.8: SEM images of M4 - M6 samples.

Table 3.4. Film thickness of MoO_3 thin films at different annealing temperatures.

Na-glass / MoO_3

Thermal vacuum evaporation, $3 \cdot 10^{-7}$ Bar, 10 min, 19 A

Sample name	Temperature, °C	film thickness, nm
M1	as-dep	1459
M2	150	1348
M3	200	1254
M4	300	1165
M5	400	645
M6	500	469

3.6 J-V characteristics of solar cells

To ascertain the performance of vacuum thermal deposited MoO_3 thin films as interfacial buffer layer for hybrid solar cells, the J-V curve measurements was carried out. The reference solar cell and the solar cell containing MoO_3 films are denoted as ITO/TiO_2/Sb_2S_3/P3HT/Au and ITO/TiO_2/ Sb_2S_3/P3HT/MoO_3/Au respectively. For both solar cells the anode material is ITO while Au is the cathode material. Figure 3.9 illustrates the diagram of both solar cells placed in one substrate (picture taken from the laboratory). The region with deposited MoO_3 is marked with a red square. It should be noted that the MoO_3 film used here is the as deposited film (M1). Also, it is noteworthy to revise that the purpose of this study is to prepare the MoO_3 thin films and evaluate the performance when placed in a real hybrid solar as an interfacial buffer layer. The performance is evaluated by taken J-V measurements and compared with that of the reference without MoO_3 films. The J-V curve measurements is presented in figure 3.9.

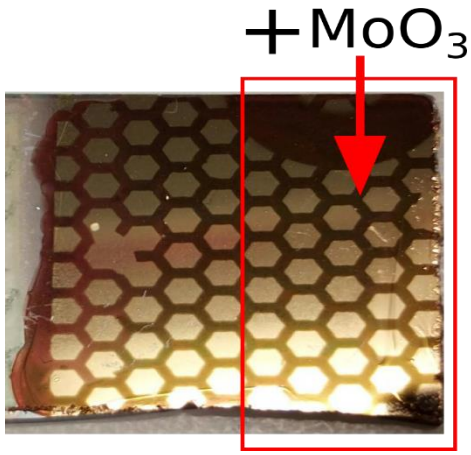

Figure 3.8: Pictures of both ITO/TiO_2/Sb_2S_3/P3HT/Au and ITO/TiO_2/Sb_2S_3/P3HT/MoO_3/Au hybrid solar cells (Picture taken from the laboratory).

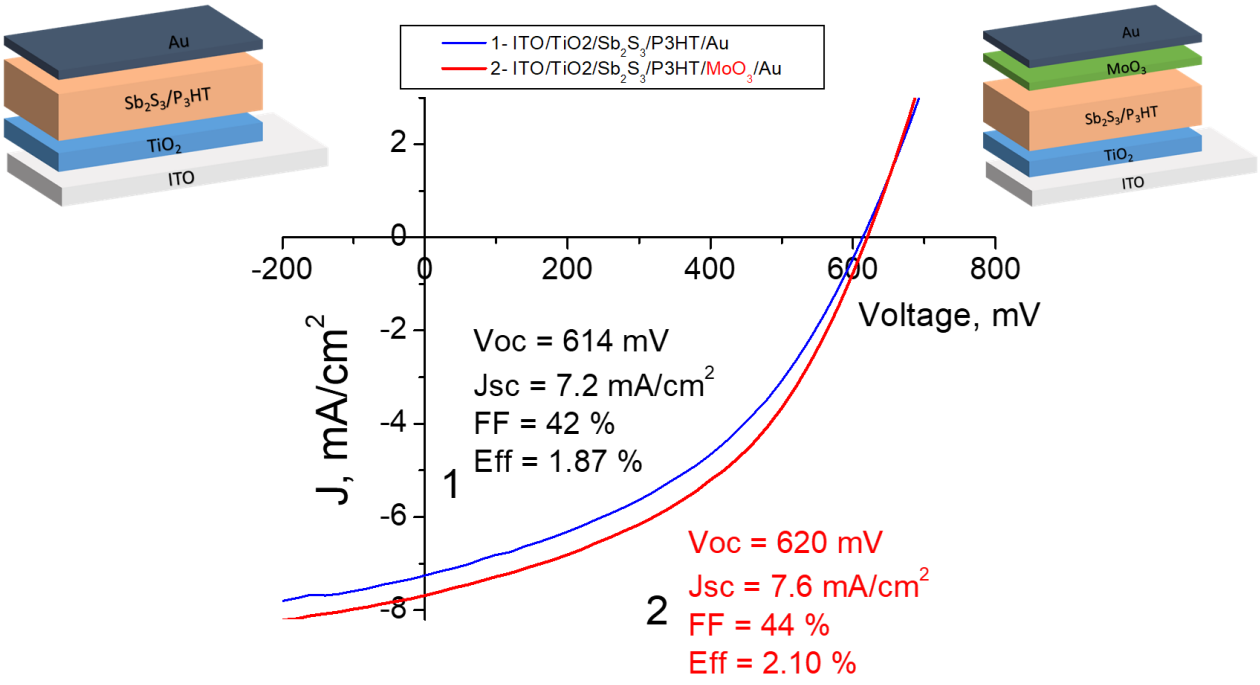

Figure 3.9: J-V measurements for both ITO/TiO_2/Sb_2S_3/P3HT/Au and ITO/TiO_2/Sb_2S_3/P3HT/MoO_3/Au hybrid solar cells.

J-V curve measurements for the reference ITO/TiO_2/Sb_2S_3/P3HT/Au solar cells shows that the open circuit voltage (Voc), short circuit current density (Jsc), Fill factor (FF) and power conversion efficiency (PCE) values are 614 mV, 7.2 mA/cm^2, 42 % and 1.87 % respectively. On the contrary, hybrid solar cell with the as- deposited MoO_3 films shows improved performance. Improved PCE value of 2.1% is achieved compared to the reference solar cell. The Voc, Jsc, FF values of also shows an improvement when compared to the reference ITO/TiO_2/Sb_2S_3/P_3HT/Au solar cell. Consequently, we propose that the as-deposited MoO_3 film is a good interfacial material for an inverted hybrid solar cell.

Chapter IV: Conclusions and Recommendations for future work

4.1 Conclusions

The main objective of this research is to study the structural and optical properties of MoO_3 thin films as interfacial buffer layer for hybrid solar cells. MoO_3 does not only acts as a protective layer against environmental oxygen and humidity but also prevents charge recombination at the electrodes thereby prolonging the lifetime and improving the output parameters of the solar cell. A good understanding of the structural and optical properties could help improve the performance and lifetime of the solar cells. MoO_3 films were deposited on glass substrates using vacuum thermal evaporation and the films are characterized by optical measurements, XRD, EDX and SEM. The as-deposited MoO_3 thin film is then used as an interfacial layer for a hybrid solar cell (ITO/TiO_2/Sb_2S_3/P3HT/MoO_3/Au) and the J-V characteristics is compared with that of a reference solar cell (ITO/TiO_2/Sb_2S_3/P3HT/ Au).

The key findings obtained from this study are highlighted below:

- The as-deposited films were amorphous although at temperatures above 200°C the degree of crystallinity of the films starts increasing.
- MoO_3 is a wide band gap semiconductor, below the crystalline temperature the band gap decreases with increasing temperature. However, the energy band gap would start to increase after heating beyond the crystalline offset temperature.
- The offset crystalline temperature of MoO_3 films is above 200°C.
- The as deposited MoO_3 samples is identified with a blue color and the blue color darkens with temperature. However, above the offset crystalline temperature the transparency of the films increases with temperature.
- Optical band gap of amorphous MoO_3 film is 3.1 eV which increases to 3.49 eV upon crystallization.
- Physical appearance also illustrates the unique ability of MoO_3 to exist in multiple valence states.
- The optical properties (reflectance), Eg and transparency of the MoO_3 thin film is largely dependent on the deposition techniques used and the thermal annealing medium.
- Crystallinity of the MoO_3 thin films does not depend on the deposition method and heating medium. But it is dependent on the thermal annealing temperature.

- There is a possible increase in the number of defects present in each crystal as the annealing temperature increases.
- Thermal treatment changes the crystalline structure of the material, but its chemical composition still remains unchanged.
- SEM results shows that with increasing annealing temperature the films thickness decreases progressively.
- The hybrid solar cells fabricated with as-deposited MoO_3 films as an interfacial buffer layer shows improved performance when compared to the standard hybrid solar cell without the MoO_3 films. PCE value increases from 1.87% to 2.1%. Voc, Jsc and FF values also shows significant increase. Therefore, the amorphous as-deposited MoO_3 films are suitable as an interfacial buffer layer for the solar cell.

4.2 Recommendations for future work

The current research has established that the use of vacuum thermal evaporated MoO_3 films as interfacial buffer layer for hybrid solar cells could improve the performance of the solar cell. However, it is only the as-deposited MoO_3 film that was tested as interfacial material (ETL) for hybrid solar cell. The following recommendation are useful for future research in this field:

1. It is recommended that other thermal annealed MoO_3 films should be tested to ascertain the effect of thermal annealing of MoO_3 films on the performance of hybrid solar cell.
2. It is also recommended to produce MoO_3 films with different thickness and test their performance in a typical hybrid solar cell.
3. Compare the effect of the method of fabrication on the performance of MoO_3 as interfacial material in hybrid solar cells.

SUMMARY

Increasing world energy demand, the finite nature of fossil fuels and the issues of climate change has intensified the search for renewable, environmentally benign and sustainable energy sources of which photovoltaics (PV) solar cell is an attractive example. The early years of PV solar cell devices was dominated by silicon solar cells due to their availability, excellent power conversion efficiencies and environmental stability. However, they are expensive in terms of purifying and manufacturing techniques. In order to compete with fossil fuels the cost of renewable energies needs to be reduced.

Hybrid solar cells provides a cheap alternative to conventional solar cells by combining organic and inorganic materials, in that way, the benefits of both materials can be utilized. However, hybrid solar cells are faced with the challenges of low efficiency and life time. Interfacial buffer layers are used to increase the efficiency and lifetime of hybrid solar cells. They smoothen the anode surface, acts as protective layers against atmospheric oxygen and humidity and minimizes charge recombination and the resistance at the interface between the anode and the photoactive layers of hybrid solar cells.

Molybdenum oxide (MoO_3) is a promising material as interfacial layers for hybrid solar cells due to its unique optical, structural and electronic properties. However, to use this material effectively it is important to understand the structural and optical properties of MoO_3 thin films which is the main aim of this study. This research also attempts to investigate the effect of thermal annealing on the structure and properties of MoO_3 thin film as interfacial buffer layers for hybrid solar cells.

Thin films MoO_3 were prepared by Vacuum thermal evaporation method on glass substrates using powdered MoO_3. The samples of MoO_3 were heated in a vacuum evaporator and then evaporated using Molybdenum (Mo) boat at 19 Amperes from 2 seconds to 10 minutes depending on the thickness of the glass. Prepared thin films were made to undergo thermal annealing temperatures of 150, 200, 300, 400 and 500 ^oC after which they are characterized by Optical transmittance, XRD, SEM, EDX. Furthermore, the performance of the as-deposited MoO_3 film as a buffer layer is evaluated in a real inverted hybrid solar cell with configuration ITO/TiO_2/Sb_2S_3/P3HT/MoO_3/Au against a reference ITO/TiO_2/Sb_2S_3/P3HT/ /Au solar cell.

Result of MoO_3 thin films on glass substrate shows that the as-deposited thin films are amorphous and at temperatures above 200°C crystallinity starts increasing. The optical properties (reflectance), band gap and transparency of the MoO_3 thin film is largely dependent on the deposition techniques used and the thermal annealing medium used. On the contrary, Crystallinity of the MoO_3 thin films is only

dependent on the thermal annealing temperatures. One important observation is the fact that thermal treatment changes the crystalline structure of the material, but its chemical composition still remains unchanged. The performance of the as-deposited MoO_3 film on hybrid solar cell shows an improvement in the power conversion efficiency (PCE)(1.87% to 2.1%), Open circuit voltage (Voc) (614 mV to 620 mV), and fill factor (FF) (42% to 44%) and short circuit current (J_{SC}) (7.2 mA/cm^2 to 7.6 mA/cm^2) . The results obtained from this study shows that the amorphous as- deposited MoO_3 thin films prepared by vacuum thermal evaporation can be effectively used to improve the efficiency and performance of a hybrid solar cell. For further studies it is recommended to investigate the effect of thermal annealing of MoO_3 thin films on the performance of hybrid solar.

List of References

[1] Y. Kumar, J. Ringenberg, S.S. Depuru, V.K. Devabhaktuni, J.W. Lee, E. Nikolaidis, B. Andersen, A. Afjeh, Wind energy: Trends and enabling technologies, Renew. Sustain. Energy Rev. 53 (2016) 209–224. doi:10.1016/j.rser.2015.07.200.

[2] E. Kabir, P. Kumar, S. Kumar, A.A. Adelodun, K.-H. Kim, Solar energy: Potential and future prospects, Renew. Sustain. Energy Rev. 82 (2018) 894–900. doi:10.1016/J.RSER.2017.09.094.

[3] J. Holm-Nielsen, E. Ehimen, Biomass supply chains for bioenergy and biorefining, 2016. https://books.google.com/books?hl=en&lr=&id=Xd_lBwAAQBAJ&oi=fnd&pg=PP1&dq=%22Biomass+supply+chains+for+bioenergy+and+biorefining%22++%22J.+Holm-Nielsen%22++%22E.A.+Ehimen%22&ots=T5q_z5m4Xq&sig=uO4VOEVa4tS9he4PmtuQ4C5dqps (accessed May 16, 2018).

[4] T. Blaschke, M. Biberacher, S. Gadocha, I. Schardinger, "Energy landscapes": Meeting energy demands and human aspirations., Biomass Bioenergy. 55 (2013) 3–16. doi:10.1016/j.biombioe.2012.11.022.

[5] A. Blakers, N. Zin, K.R. McIntosh, K. Fong, High efficiency silicon solar cells, Energy Procedia. 33 (2013) 1–10. doi:10.1016/j.egypro.2013.05.033.

[6] M.A. Green, Third generation photovoltaics: solar cells for 2020 and beyond, Phys. E Low-Dimensional Syst. Nanostructures. 14 (2002) 65–70. doi:10.1016/S1386-9477(02)00361-2.

[7] A.M. Hermann, Polycrystalline thin-film solar cells – A review, Sol. Energy Mater. Sol. Cells. 55 (1998) 75–81. doi:10.1016/S0927-0248(98)00048-8.

[8] M. Bhogaita, A.D. Shukla, R.P. Nalini, Recent advances in hybrid solar cells based on natural dye extracts from Indian plant pigment as sensitizers, Sol. Energy. 137 (2016) 212–224. doi:10.1016/J.SOLENER.2016.08.003.

[9] M.A. Green, Third Generation Photovoltaics: Advanced Solar Energy Conversion - Martin A. Green - Google Books, 2006. https://books.google.ca/books?hl=en&lr=&id=21VSH1YIWTQC&oi=fnd&pg=PA1&dq=1.%09Green,+Martin+A.+Third+generation+photovoltaics.+New+York:+Springer,+2006.&ots=5v9dshLJD-

&sig=Y9XaVdk2S3f0trEfEMqD9OqTImI#v=onepage&q=1.%09Green%2C Martin A. Third gener (accessed March 26, 2018).

[10] S. Günes, N.S. Sariciftci, Hybrid solar cells, Inorganica Chim. Acta. 361 (2008) 581–588. doi:10.1016/j.ica.2007.06.042.

[11] F.C. Krebs, Fabrication and processing of polymer solar cells: A review of printing and coating techniques, Sol. Energy Mater. Sol. Cells. 93 (2009) 394–412. doi:10.1016/J.SOLMAT.2008.10.004.

[12] T.T. Larsen-Olsen, B. Andreasen, T.R. Andersen, A.P.L. Böttiger, E. Bundgaard, K. Norrman, J.W. Andreasen, M. Jørgensen, F.C. Krebs, Simultaneous multilayer formation of the polymer solar cell stack using roll-to-roll double slot-die coating from water, Sol. Energy Mater. Sol. Cells. 97 (2012) 22–27. doi:10.1016/j.solmat.2011.08.026.

[13] M. Wright, A. Uddin, Organic-inorganic hybrid solar cells: A comparative review, Sol. Energy Mater. Sol. Cells. 107 (2012) 87–111. doi:10.1016/j.solmat.2012.07.006.

[14] E. Voroshazi, B. Verreet, A. Buri, R. Müller, D. Di Nuzzo, P. Heremans, Influence of cathode oxidation via the hole extraction layer in polymer:fullerene solar cells, Org. Electron. Physics, Mater. Appl. 12 (2011) 736–744. doi:10.1016/j.orgel.2011.01.025.

[15] M. Wang, M. Zhou, L. Zhu, Q. Li, C. Jiang, ScienceDirect Enhanced polymer solar cells efficiency by surface coating of the PEDOT : PSS with polar solvent, Sol. Energy. 129 (2016) 175–183. doi:10.1016/j.solener.2016.02.003.

[16] T. Stubhan, T. Ameri, M. Salinas, J. Krantz, F. MacHui, M. Halik, C.J. Brabec, High shunt resistance in polymer solar cells comprising a MoO3 hole extraction layer processed from nanoparticle suspension, Appl. Phys. Lett. 98 (2011) 253308. doi:10.1063/1.3601921.

[17] J. Liu, S. Shao, G. Fang, B. Meng, Z. Xie, L. Wang, High-efficiency inverted polymer solar cells with transparent and work-function tunable MoO3-Al composite film as cathode buffer layer, Adv. Mater. 24 (2012) 2774–2779. doi:10.1002/adma.201200238.

[18] B.J. Worfolk, T.C. Hauger, K.D. Harris, D.A. Rider, J.A.M. Fordyce, S. Beaupré, M. Leclerc, J.M. Buriak, Work function control of interfacial buffer layers for efficient and air-stable inverted low-bandgap organic photovoltaics, Adv. Energy Mater. 2 (2012) 361–368.

doi:10.1002/aenm.201100714.

[19] S.K. Hau, H.-L. Yip, A.K.-Y. Jen, A Review on the Development of the Inverted Polymer Solar Cell Architecture, Polym. Rev. 50 (2010) 474–510. doi:10.1080/15583724.2010.515764.

[20] T. Yang, W. Cai, D. Qin, E. Wang, L. Lan, X. Gong, J. Peng, Y. Cao, Solution-Processed Zinc Oxide Thin Film as a Buffer Layer for Polymer Solar Cells with an Inverted Device Structure, (n.d.). doi:10.1021/jp1003984.

[21] G. Li, C.-W. Chu, V. Shrotriya, J. Huang, Y. Yang, Efficient inverted polymer solar cells, Appl. Phys. Lett. 88 (2006) 253503. doi:10.1063/1.2212270.

[22] A.K. Prasad, D.J. Kubinski, P.I. Gouma, Comparison of sol–gel and ion beam deposited MoO3 thin film gas sensors for selective ammonia detection, Sensors Actuators B Chem. 93 (2003) 25–30. doi:10.1016/S0925-4005(03)00336-8.

[23] Kouta Hosono, * Ichiro Matsubara, Norimitsu Murayama, and Shin Woosuck, N. Izu, Synthesis of Polypyrrole/MoO3 Hybrid Thin Films and Their Volatile Organic Compound Gas-Sensing Properties, (2004). doi:10.1021/CM0492641.

[24] K. Gesheva, A. Szekeres, T. Ivanova, Optical properties of chemical vapor deposited thin films of molybdenum and tungsten based metal oxides, Sol. Energy Mater. Sol. Cells. 76 (2003) 563–576. doi:10.1016/S0927-0248(02)00267-2.

[25] V. Bhosle, A. Tiwari, J. Narayan, Epitaxial growth and properties of MoOx(2<x<2.75) films, J. Appl. Phys. 97 (2005) 83539. doi:10.1063/1.1868852.

[26] N. Illyaskutty, S. Sreedhar, H. Kohler, R. Philip, V. Rajan, V.P.M. Pillai, ZnO-modified MoO3 nano-rods, -wires, -belts and -tubes: Photophysical and nonlinear optical properties, J. Phys. Chem. C. 117 (2013) 7818–7829. doi:10.1021/jp311394y.

[27] H. Zeng, X. Zhu, Y. Liang, X. Guo, Interfacial layer engineering for performance enhancement in polymer solar cells, Polymers (Basel). 7 (2015) 333–372. doi:10.3390/polym7020333.

[28] S.S. Mahajan, S.H. Mujawar, P.S. Shinde, a I. Inamdar, P.S. Patil, Concentration Dependent Structural , Optical and Electrochromic Properties of MoO 3 Thin Films, Int. J. Electrochem. Sci. 3 (2008) 953–960. www.electrochemsci.org (accessed May 14, 2018).

[29] T. Dittrich, Materials Concepts for Solar Cells, IMPERIAL COLLEGE PRESS, 2014. doi:10.1142/p937.

[30] A. McEvoy, T. Markvart, L. Castañer, T. Markvart, Practical handbook of photovoltaics: fundamentals and applications, 2003. https://books.google.ca/books?hl=en&lr=&id=E2BAosEwDfQC&oi=fnd&pg=PP1&dq=7.%09McEvoy,+Augustin,+et+al.,+eds.+Practical+handbook+of+photovoltaics:+fundamentals+and+applications.+Elsevier,+2003.&ots=HNsYlGXDMi&sig=x6Yshz7yCy7r_qIwNQ6ny5T61BU (accessed May 1, 2018).

[31] M.A. Green, Photovoltaics: technology overview, Energy Policy. 28 (2000) 989–998. doi:10.1016/s0301-4215(00)00086-0.

[32] C. a. Angell, Glass Transition, Encycl. Mater. Sci. Technol. 4 (2001) 3565–3575. http://www.public.asu.edu/~caangell/381_Angell_Glass.pdf (accessed May 1, 2018).

[33] L.L. Kazmerski, Solar photovoltaics R&D at the tipping point: A 2005 technology overview, J. Electron Spectros. Relat. Phenomena. 150 (2006) 105–135. doi:10.1016/j.elspec.2005.09.004.

[34] W.A. Badawy, A review on solar cells from Si-single crystals to porous materials and Quantum dots, J. Adv. Res. 6 (2015) 123–132. doi:10.1016/j.jare.2013.10.001.

[35] Lev I. Berger, Semiconductor Materials, CRC Press, Boca Raton, FL , 1997. https://books.google.ca/books?hl=en&lr=&id=Ty5Ymlg_Mh0C&oi=fnd&pg=PA9&dq=12.%09Berger,+1997+L.I.+Berger+Semiconductor+Materials+CRC+Press,+Boca+Raton,+FL+(1997)&ots=K6Y5sxQcUt&sig=D5vSU8tqsaoTJzCkLHA6P3hZhoI#v=onepage&q=12.%09Berger%2C 1997 L.I. Ber (accessed May 1, 2018).

[36] B. O'Regan, M. Grätzel, A low-cost, high-efficiency solar cell based on dye-sensitized colloidal TiO2 films, Nature. 353 (1991) 737–740. doi:10.1038/353737a0.

[37] W. Ghann, H. Kang, T. Sheikh, S. Yadav, T. Chavez-Gil, F. Nesbitt, J. Uddin, Fabrication, Optimization and Characterization of Natural Dye Sensitized Solar Cell, Sci. Rep. 7 (2017) 41470. doi:10.1038/srep41470.

[38] F.C. Krebs, Fabrication and processing of polymer solar cells: A review of printing and coating techniques, Sol. Energy Mater. Sol. Cells. 93 (2009) 394–412. doi:10.1016/j.solmat.2008.10.004.

[39] S. Sumaiya, K. Kardel, A. El-Shahat, Organic Solar Cell by Inkjet Printing—An Overview, Technologies. 5 (2017) 53. doi:10.3390/technologies5030053.

[40] M. Wright, A. Uddin, Organic-inorganic hybrid solar cells: A comparative review, Sol. Energy Mater. Sol. Cells. 107 (2012) 87–111. doi:10.1016/j.solmat.2012.07.006.

[41] Y. Zhou, M. Eck, M. Krüger, Bulk-heterojunction hybrid solar cells based on colloidal nanocrystals and conjugated polymers, Energy Environ. Sci. 3 (2010) 1851. doi:10.1039/c0ee00143k.

[42] S. Dayal, N. Kopidakis, D.C. Olson, D.S. Ginley, G. Rumbles, Photovoltaic Devices with a Low Band Gap Polymer and CdSe Nanostructures Exceeding 3% Efficiency, Nano Lett. 10 (2010) 239–242. doi:10.1021/nl903406s.

[43] Y. Zhou, M. Eck, M. Krüger, Organic-Inorganic Hybrid Solar Cells: State of the Art, Challenges and Perspectives, Intechopen.Com. (2011). doi:10.5772/19732.

[44] S.E. Gledhill, B. Scott, B.A. Gregg, Organic and nano-structured composite photovoltaics: An overview, J. Mater. Res. 20 (2005) 3167–3179. doi:10.1557/jmr.2005.0407.

[45] J.J.M. Halls, C.A. Walsh, N.C. Greenham, E.A. Marseglia, R.H. Friend, S.C. Moratti, A.B. Holmes, Efficient photodiodes from interpenetrating polymer networks, Nature. 376 (1995) 498–500. doi:10.1038/376498a0.

[46] B.R. Saunders, Hybrid polymer/nanoparticle solar cells: Preparation, principles and challenges, J. Colloid Interface Sci. 369 (2012) 1–15. doi:10.1016/j.jcis.2011.12.016.

[47] S. Lattante, Electron and Hole Transport Layers: Their Use in Inverted Bulk Heterojunction Polymer Solar Cells, Electronics. 3 (2014) 132–164. doi:10.3390/electronics3010132.

[48] M. Irwin, D. Buchholz, … A.H.-… N.A., undefined 2008, p-Type semiconducting nickel oxide as an efficiency-enhancing anode interfacial layer in polymer bulk-heterojunction solar cells, Natl. Acad Sci. (n.d.). http://www.pnas.org/content/105/8/2783.short (accessed May 16, 2018).

[49] V. Shrotriya, G. Li, Y. Yao, C.-W. Chu, Y. Yang, Transition metal oxides as the buffer layer for polymer photovoltaic cells, Appl. Phys. Lett. 88 (2006) 73508. doi:10.1063/1.2174093.

[50] C.-W. Chu, S.-H. Li, C.-W. Chen, V. Shrotriya, Y. Yang, High-performance organic thin-film transistors with metal oxide/metal bilayer electrode, Appl. Phys. Lett. 87 (2005) 193508. doi:10.1063/1.2126140.

[51] S. Tokito, K. Noda, Y. Taga, Metal oxides as a hole-injecting layer for an organic electroluminescent device, J. Phys. D. Appl. Phys. 29 (1996) 2750–2753. doi:10.1088/0022-

3727/29/11/004.

[52] E. Voroshazi, B. Verreet, … T.A.-S.E.M., undefined 2011, Long-term operational lifetime and degradation analysis of P3HT: PCBM photovoltaic cells, Elsevier. (n.d.). https://www.sciencedirect.com/science/article/pii/S0927024810005295 (accessed May 16, 2018).

[53] C. Dwivedi, T. Mohammad, V. Bharti, A. Patra, S. Pathak, V. Dutta, CoSP approach for the synthesis of blue MoO3 nanoparticles for application as hole transport layer (HTL) in organic solar cells, Sol. Energy. 162 (2018) 78–83. doi:10.1016/J.SOLENER.2017.12.063.

[54] A. Bouzidi, N. Benramdane, H. Tabet-Derraz, C. Mathieu, B. Khelifa, R. Desfeux, Effect of substrate temperature on the structural and optical properties of MoO3thin films prepared by spray pyrolysis technique, Mater. Sci. Eng. B Solid-State Mater. Adv. Technol. 97 (2003) 5–8. doi:10.1016/S0921-5107(02)00385-9.

[55] B. K., Colouration of tungsten oxide fillms: A model for optically active coatings, Sol. Energy Mater. Sol. Cells. 58 (1999) 1–131. https://scholar.google.ca/scholar?hl=en&as_sdt=0%2C5&q=Colouration+of+tungsten+oxide+%22lms%3A+A+model+for+optically+active+coatings&btnG= (accessed May 14, 2018).

[56] L. Boudaoud, N. Benramdane, R. Desfeux, B. Khelifa, C. Mathieu, Structural and optical properties of MoO3and V2O5thin films prepared by Spray Pyrolysis, Catal. Today. 113 (2006) 230–234. doi:10.1016/j.cattod.2005.11.072.

[57] T.H. Lai, S.W. Tsang, J.R. Manders, S. Chen, F. So, Properties of interlayer for organic photovoltaics, Mater. Today. 16 (2013) 424–432. doi:10.1016/j.mattod.2013.10.001.

[58] R. Po, C. Carbonera, A. Bernardi, N. Camaioni, The role of buffer layers in polymer solar cells, Energy Environ. Sci. 4 (2011) 285–310. doi:10.1039/C0EE00273A.

[59] X. Guo, T.J. Marks, Plastic solar cells with engineered interfaces, in: C.E. Tabor, F. Kajzar, T. Kaino, Y. Koike (Eds.), Spie Opto, International Society for Optics and Photonics, 2013: p. 86220K. doi:10.1117/12.2013491.

[60] R.S. Mane, C.D. Lokhande, Chemical deposition method for metal chalcogenide thin films, Mater. Chem. Phys. 65 (2000) 1–31. doi:10.1016/S0254-0584(00)00217-0.

[61] P.S. Patil, Versatility of chemical spray pyrolysis technique, Mater. Chem. Phys. 59 (1999) 185–198. doi:10.1016/S0254-0584(99)00049-8.

[62] Z. Xiao, Q. Dong, C. Bi, Y. Shao, Y. Yuan, J. Huang, Solvent Annealing of Perovskite-Induced Crystal Growth for Photovoltaic-Device Efficiency Enhancement, Adv. Mater. 26 (2014) 6503–6509. doi:10.1002/adma.201401685.

[63] U.A. Charles, M.A. Ibrahim, M.A.M. Teridi, Electrodeposition of organic–inorganic tri-halide perovskites solar cell, J. Power Sources. 378 (2018) 717–731. doi:10.1016/j.jpowsour.2017.12.075.

[64] Y. Xiao, G. Han, J. Wu, J.-Y. Lin, Efficient bifacial perovskite solar cell based on a highly transparent poly(3,4-ethylenedioxythiophene) as the p-type hole-transporting material, J. Power Sources. 306 (2016) 171–177. doi:10.1016/J.JPOWSOUR.2015.12.003.

[65] D. Mattox, Handbook of Physical Vapor Deposition (PVD), 2010. https://books.google.ca/books?hl=en&lr=&id=aGUxoVTYjA8C&oi=fnd&pg=PP1&dq=Handbook+of+Physical+Vapor+Deposition+(PVD)+Processing+(Second+Edition)+2010,+Pages+195–235+++Cover+image+Chapter+6+–+Vacuum+Evaporation+and+Vacuum+Deposition&ots=bWrY789O1u&sig=bN3U (accessed May 16, 2018).

[66] B. Hu, L. Mai, W. Chen, F. Yang, From MoO3 nanobelts to MoO2 nanorods: structure transformation and electrical transport., ACS Nano. 3 (2009) 478–482. doi:10.1021/nn800844h.

[67] K.S. Rao, K.V. Madhuri, S. Uthanna, O.M. Hussain, C. Julien, Photochromic properties of double layer CdS/MoO3 nano-structured films, Mater. Sci. Eng. B. 100 (2003) 79–86. doi:10.1016/S0921-5107(03)00078-3.

[68] S.-Y. Lin, Y.-C. Chen, C.-M. Wang, P.-T. Hsieh, S.-C. Shih, Post-annealing effect upon optical properties of electron beam evaporated molybdenum oxide thin films, Appl. Surf. Sci. 255 (2009) 3868–3874. doi:10.1016/J.APSUSC.2008.10.069.

[69] T.S. Sian, G.B. Reddy, Optical, structural and photoelectron spectroscopic studies on amorphous and crystalline molybdenum oxide thin films, Sol. Energy Mater. Sol. Cells. 82 (2004) 375–386. doi:DOI 10.1016/j.solmat.2003.12.007.

[70] S.-Y. Lin, Y.-C. Chen, C.-M. Wang, P.-T. Hsieh, S.-C. Shih, Post-annealing effect upon optical properties of electron beam evaporated molybdenum oxide thin films, Appl. Surf. Sci. 255 (2009) 3868–3874. doi:10.1016/j.apsusc.2008.10.069.

[71] A. Boukhachem, C. Bouzidi, R. Boughalmi, R. Ouerteni, M. Kahlaoui, B. Ouni, H. Elhouichet, M. Amlouk, Physical investigations on MoO3sprayed thin film for selective sensitivity applications, Ceram. Int. 40 (2014) 13427–13435. doi:10.1016/j.ceramint.2014.05.062.

[72] H.R. Philipp, Optical properties of non-crystalline Si, SiO, SiOxand SiO2, J. Phys. Chem. Solids. 32 (1971) 1935–1945. doi:10.1016/S0022-3697(71)80159-2.

[73] S.Y. Lin, Y.C. Chen, C.M. Wang, P.T. Hsieh, S.C. Shih, Post-annealing effect upon optical properties of electron beam evaporated molybdenum oxide thin films, Appl. Surf. Sci. 255 (2009) 3868–3874. doi:10.1016/j.apsusc.2008.10.069.

[74] C. V. Ramana, C.M. Julien, Chemical and electrochemical properties of molybdenum oxide thin films prepared by reactive pulsed-laser assisted deposition, Chem. Phys. Lett. 428 (2006) 114–118. doi:10.1016/j.cplett.2006.06.117.

[75] A. Boukhachem, C. Bouzidi, R. Boughalmi, R. Ouerteni, M. Kahlaoui, B. Ouni, H. Elhouichet, M. Amlouk, Physical investigations on MoO3 sprayed thin film for selective sensitivity applications, Ceram. Int. 40 (2014) 13427–13435. doi:10.1016/j.ceramint.2014.05.062.

[76] H.M. Martínez, J. Torres, L.D. López Carreño, M.E. Rodríguez-García, Effect of the substrate temperature on the physical properties of molybdenum tri-oxide thin films obtained through the spray pyrolysis technique, Mater. Charact. 75 (2013) 184–193. doi:10.1016/j.matchar.2012.11.002.

[77] R. Tripathi, A. Kumar, C. Bharti, T.P. Sinha, Dielectric relaxation of ZnO nanostructure synthesized by soft chemical method, Curr. Appl. Phys. 10 (2010) 676–681. doi:10.1016/j.cap.2009.08.015.

[78] R. Boughalmi, A. Boukhachem, I. Gaied, K. Boubaker, M. Bouhafs, M. Amlouk, Effect of tin content on the electrical and optical properties of sprayed silver sulfide semiconductor thin films, Mater. Sci. Semicond. Process. 16 (2013) 1584–1591. doi:10.1016/j.mssp.2013.05.019.

[79] A. Guerfi, Characterization and Stability of Electrochromic MoO[sub 3] Thin Films Prepared by Electrodeposition, J. Electrochem. Soc. 142 (1995) 3457. doi:10.1149/1.2050004.

[80] C.S. Hsu, C.C. Chan, H.T. Huang, C.H. Peng, W.C. Hsu, Electrochromic properties of nanocrystalline MoO3 thin films, Thin Solid Films. 516 (2008) 4839–4844. doi:10.1016/j.tsf.2007.09.019.

Appendices

A1: Optical Properties

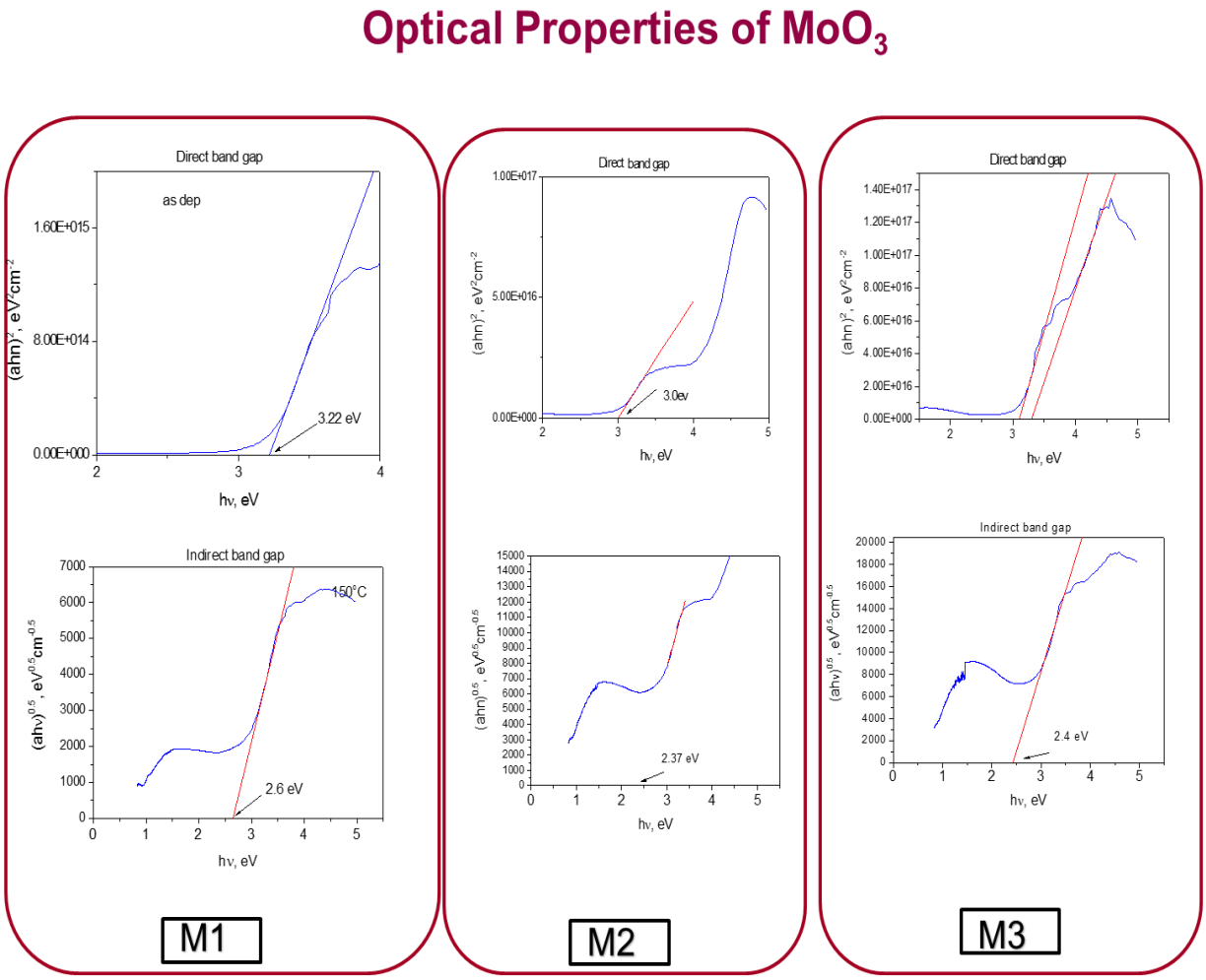

Optical Properties of MoO_3

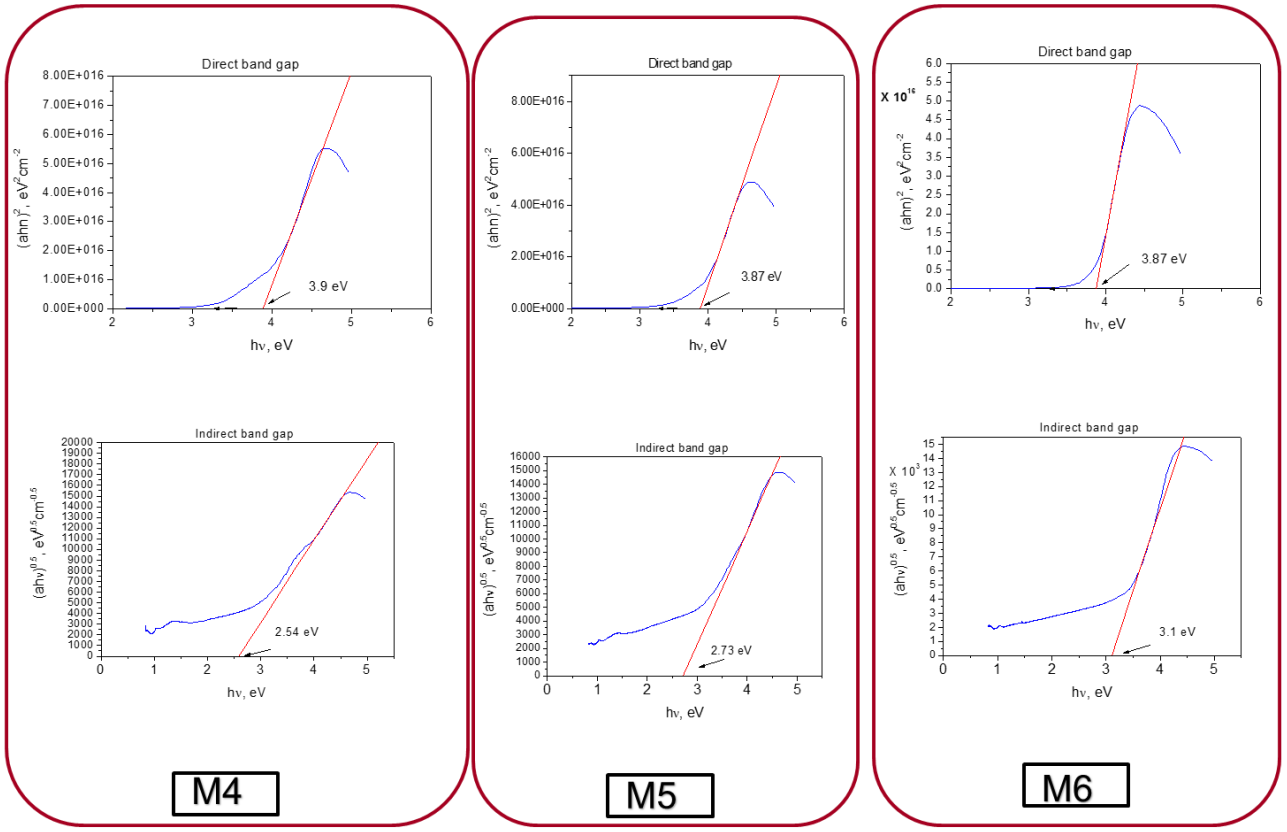

A2: XRD patterns

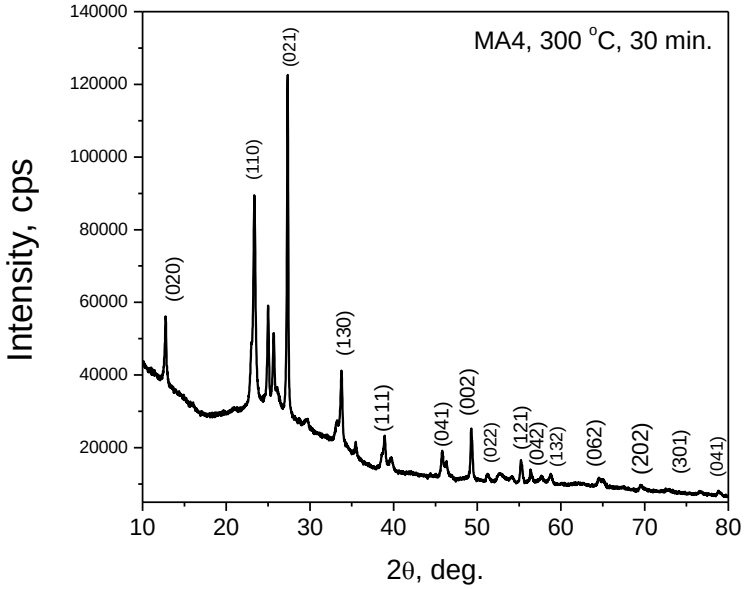

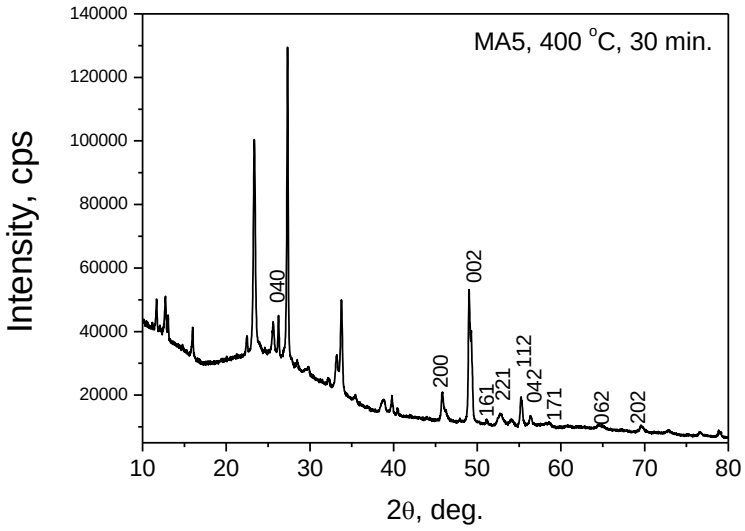

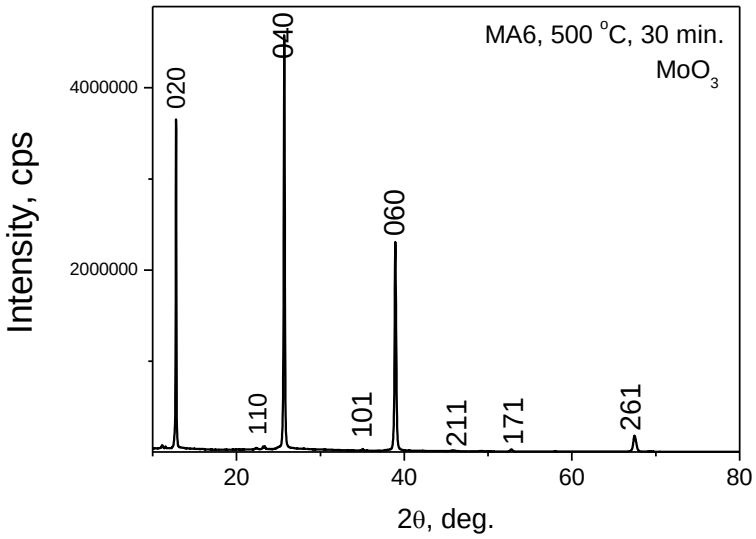
MA6, 500 °C, 30 min.
MoO3
Intensity, cps
4000000
2000000
020
040
060
110
101
211
171
261
20
40
60
80
2θ, deg.